REPORT DOCUMENTATION PAGE

Form Approved
OMB No. 0704-0188

1. REPORT DATE *(DD-MM-YYYY)*	**2. REPORT TYPE**	**3. DATES COVERED** *(From - To)*
01-11-2017	Report CLIN0003	28 Oct 2016 to 11 Jan 2017

4. TITLE AND SUBTITLE
Imaging through fog using polarization imaging in the Visible/NIR/SWIR spectrum

5a. CONTRACT NUMBER
N00014-16-P-2035

5b. GRANT NUMBER n/a

5c. PROGRAM ELEMENT NUMBER n/a

6. AUTHOR(S)
BREUGNOT, Sebastien
EL KETARA, Mohamed

5d. PROJECT NUMBER n/a

5e. TASK NUMBER n/a

5f. WORK UNIT NUMBER n/a

7. PERFORMING ORGANIZATION NAME(S) AND ADDRESS(ES)
Bossa Nova Technologies, LLC
11922 Jefferson Blvd
Culver city, CA 90230

8. PERFORMING ORGANIZATION REPORT NUMBER
0001

9. SPONSORING/MONITORING AGENCY NAME(S) AND ADDRESS(ES) Office of Naval Research
875 North Randolph Street
Arlington VA 22203

10. SPONSOR/MONITOR'S ACRONYM(S) n/a

11. SPONSORING/MONITORING AGENCY REPORT NUMBER 001

12. DISTRIBUTION AVAILABILITY STATEMENT
Approved for public release. Distribution is unlimited.

13. SUPPLEMENTARY NOTES
n/a

14. ABSTRACT

15. SUBJECT TERMS Imaging through fog, polarization					
16. SECURITY CLASSIFICATION OF:			17. LIMITATION OF ABSTRACT SAR	18. NUMBER OF PAGES 47	19a. NAME OF RESPONSIBLE PERSON S.Breugnot
a. REPORT U	b. ABSTRACT U	c. THIS PAGE U			19b. TELEPHONE NUMBER (*Include area code)* (310) 577-8113

Standard Form 298 (Rev. 8-98)
Prescribed by ANSI-Std Z39-18

Table of Contents

1 Executive Summary

This Phase I effort sought to develop a passive, electric-optical and infrared (EO-IR) imaging system. This system employs jointly optimized multi-modal image acquisition and processing methods in order to increase the operational range (the distance between the sensor and the object/scene of interest) by 10X over a baseline range that corresponds to traditional, single-mode image acquisition in the presence of obscurants. Because the gain in image quality associated with a single optimization technique may be modest, a multi-modal hardware solution combined with coordinated processing techniques was tested during this effort in order to achieve an exponentially more substantial improvement.

In order to validate this concept, we first developed a model of the interaction between light and the scattering particles present in the obscurant. In the meantime, a laboratory setup was built to validate experimentally this model and adjust our dehazing approach.

The dehazing solution obtained combines smart image acquisition and post processing methods. It is performed in three successive steps: spectral selection (acquisition), polarization modulation (acquisition) and image filtering (post-processing).

Several outdoors measurements were conducted with a polarization imaging camera operating in the visible spectrum in order to validate the approached described above. Further work has also been conducted in the Short Wave Infrared (SWIR) spectrum. A Phase IB and Phase II effort will extend this effort.

2 Project main Objective

The main goal of this Phase 1 effort was to determine the feasibility and design of a multi-modal EO-IR system with jointly optimized sensing and processing techniques that could achieve a 10X improvement in operational range compared to single-mode operation in the presence of obscurant.

3 Project Approach

The approach selected to reach this objective is based on the excellent performance of the existing passive full Stokes polarization imaging camera for visible light "SALSA" (developed by Bossa Nova Technologies DoD Phase II SBIR: W56HZV-05-C-0646), coupled with that of a SWIR (Short Wave Infrared) camera. The selected design combines a polarization imaging camera operating in the visible-NIR (Near Infrared) range with a polarization imaging camera operating in the SWIR (Short Wave Infrared) spectral band.

To validate the proposed approach, the Phase 1 effort was composed of:

- Task1: Assembly of a laboratory setup (completed)
- Task2: Development of the scattering model (completed)
- Task3: Processing development for the visible polarimetric camera software (completed)
- Task4: Characterization of the visible light polarimetric system efficiency (completed)
- Task5: SWIR camera for imaging through haze (completed)
- Task6: Study of the performance and characterization of the SWIR camera and the polarimetric visible light range camera (completed)

The results obtained during this Phase I effort are presented in five different sections which have been completed throughout the course of those tasks:

- **The physical model of interaction light/particles (Task2)**
  This section describes the model of interaction between light and the scattering particles. The simulation results obtained are detailed, particularly the spectral dependency and effects on the polarization of light. It also highlights how the comprehension of these interactions lead to a solution based on a multispectral, polarization imaging system.
- **A Multispectral polarization imaging solution (Task3)**
  In this section, the steps leading to image dehazing are detailed. Specific question are addressed such as: what polarization modulation should be used to obtain the highest dehazing effect? What is the image processing principle? This solution is evaluated using various testing environments.
- **The Testing environment (Task1)**
  In this section, controlled and uncontrolled environments used to evaluate the efficiency of the solution proposed are introduced. A quick introduction on evaluation techniques challenges is also presented.
- **The results on controlled environment (Task3+4)**

This section details the dehazing results obtained with the polarimetric visible camera using the laboratory setup developed in task2. In order to quantitatively report the dehazing effect, one evaluation technique is introduced.

- **The results on non-controlled environment (Task5+6)**
  This section details the dehazing results obtained with the polarimetric visible camera and the SWIR camera on the field. Another method to quantify the dehazing effect is introduced.

3.1 Physical model of interaction light/particles

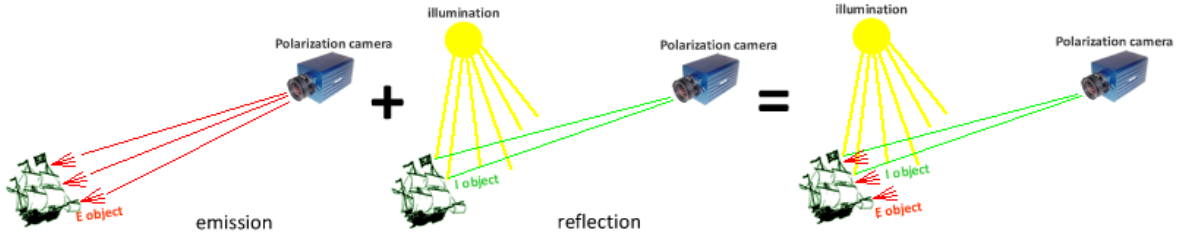

Figure 1: Schematic representation of the interaction of light on clear day

During a clear day, an imaging system can collect principally two light components (figure 1):

$$I_{detect}(x, y, \lambda, \theta, \varphi) = I_{object}(x, y, \lambda, \theta, \varphi) + E_{object}(x, y, \lambda, \theta, \varphi) \quad (1)$$

$I_{detect}(x, y, \lambda, \theta, \varphi)$ the light impinging on the camera
$I_{object}(x, y, \lambda, \theta, \varphi)$ the light from the sun reflected by the object towards the camera direction
$E_{object}(x, y, \lambda, \theta, \varphi)$ the light emitted/radiated spontaneously by the target object
(x, y) the pixel coordinates of the scene,
λ the wavelength of light observed using the camera,
(θ, φ) the angles in spherical coordinates of light illumination

During a foggy day, small liquid droplets present in the air scatter the light in the atmosphere. As a result, visible light coming from the object observed is attenuated and the image observed is blurred. The ambient light path is also modified by those aerosolized particles: atmospheric light scattered by the obscurant medium combines with reflected light from the target objet causing a decrease in image contrast as well as color degradation (figure 2).

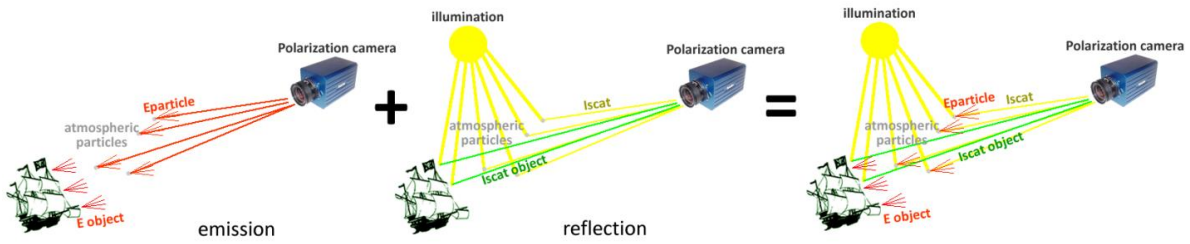

Figure 2: Schematic representation of the interaction of light with aerosolized particle during imaging

The radiative transfer equation for the intensity of light measured on the detector can be expressed as:

$$I_{detect}(x,y,\lambda,\theta,\varphi,t,z,r) = I_{scat\,[object]}(x,y,\lambda,\theta,\varphi,t,z,r) + I_{scat\,[particles]}(x,y,\lambda,\theta,\varphi,t,z,r) + E_{object\,(x,y,\lambda,\theta,\varphi,t,z,r)} + E_{particles}(x,y,\lambda,\theta,\varphi,t,z,r) \quad (2)$$

With

$I_{scat\,[object]}(x,y,\lambda,\theta,\varphi,t,z,r)$ the light coming from the object illuminated by a natural light source I_{object} which travels through the medium and is scattered by haze particles during its path towards the camera

$I_{scat\,[particles]}(x,y,\lambda,\theta,\varphi,t,z,r)$ the backscattered light also called airlight [1,2]: the light coming from the illumination source, scattered by the medium and going directly to the camera

$E_{object}(x,y,\lambda,\theta,\varphi,t,z,r)$ the light emitted/radiated by the target object

$E_{particle}(x,y,\lambda,\theta,\varphi,t,z,r)$ the light emitted/radiated by the aerosol particles located between the object and the sensor

(t,z,r) are the scattering medium characteristics. They are respectively the medium transmission, the haze depth and the particle size.

In most cases, the light spontaneously emitted by the observed object and by the aerosol particles is the result of thermal radiations. The wavelength of the light emitted depends on the temperature and can be calculated using Planck's law of black-body radiation [3]. Using the Wien's approximation, the maximum wavelength peak of this radiation λ is given by

$$\lambda_{max} = \frac{b}{T} \quad (3)$$

With b the Wien's displacement constant equal to $2.898.10^{-3}$ m.K and T the temperature in Kelvin. Using this relation it is possible to estimate the typical light contribution from haze or typical passive object.

For this type of objects, the typical temperature is around 293-323K and thus, the peak radiation is mostly in the far infrared ~ 9µm.

With these considerations, Equation (3) can be simplified for the visible [400-700nm], near infrared (NIR) [700-1000nm] or short wave infrared (SWIR) [1-3um] wavelengths to the following expression:

$$I_{detect}(x,y,\lambda,\theta,\varphi,t,z,r) = I_{scat\,[object]}(x,y,\lambda,\theta,\varphi,t,z,r) + I_{scat\,[particles]}(x,y,\lambda,\theta,\varphi,t,z,r) \quad (4)$$

The goal is to estimate I_{object} with the best accuracy. In order to recover I_{object} from the intensity detected I_{detect}, it is necessary to minimize the airlight component $I_{scat\,[particles]}$ relatively to the signal of interest I_{object}.

The undesired parameter $I_{scat\ [particles]}$ does not have the same physical origin as I_{object}. Thus, scattered photons can have different dependency regarding some physical parameters (such as polarization) compared to ballistic photons directly reflected by the object.
Therefore, **the key to achieve a 10X improvement in operational range compared to single-mode operation in the presence of obscurant is to understand those dependencies**. This has been done by modeling the interaction between light and haze particle**.**

The next section introduces the model used. It details also the principal results that have been obtained through it: **the undesired parameter's amplitude depends on the light's wavelength and features a specific polarization signature.** Those results have been used to design the best imaging acquisition system possible.

3.1.1 Light scattering models

As discussed previously, the presence of aerosolized particle introduce an undesired parameter $I_{scat\ [particles]}$.This component is due to the interaction between light and haze particle: when light interacts with matter, the electromagnetic field is modified and the photons can be reradiated (scattered) by the particle towards the camera direction.
This interaction can be classified in two categories: elastic and inelastic {the elastic scattering, in contrast to the inelastic scattering, is a process in which the kinetic energy of the light is conserved}. The elastic scattering, which is detailed in this study, is the predominant effect in scattering (approximately only 1 out of 10^7photons scattered is not scattered elastically) [4].
The elastic scattering effects can be described using two different interaction models: the Rayleigh and the Mie theories. The description of the scattering process with one or the other theory is linked to the circumference of the scattering particle πD (D the diameter of the particle) and the wavelength of the incident light λ.

- $\pi D \ll \lambda$: Rayleigh scattering

In the Rayleigh scattering model, the scattering particle can be seen as an oscillating dipole induced by the light electric field. Thus, the dipole radiation pattern can be calculated (see detailed in Appendix B- Rayleigh scattering).

- $\pi D \sim \lambda$: Mie scattering

The Mie theory is a very general and complex scattering model, which describes the interaction of an electromagnetic plane wave by a single homogeneous sphere using the Maxwell equations (see detailed in Appendix B- Mie scattering). It is valid for any particle size. However, it is harder to apprehend directly the concept, which explains why the Rayleigh theory is generally preferred for small sized particles compared to wavelength.

Since Rayleigh scattering approach is an approximation of the Mie scattering model, it is therefore necessary in the general case to develop a complete Mie scattering model software to predict the haze effect on measurements (see Appendix B- Mie scattering).

In fog, the ambient medium is air with a permeability of 1.25663753×10^{-6} H/m and the haze particle is principally composed of water with a permeability of 1.256627×10^{-6} H/m [7]. Thus, we can in first approximation consider that the ratio of magnetic permeability is equal to 1.
Under that approximation, only three parameters are necessary to determine completely the scattered light field $I_{scat\,[particles]}$:

- The size of the haze particle: r = D/2
- The complex index of refraction of the haze particle: m
- The electric field of the incident light.

Note: the dependency of the scattering with the wavelength is not clearly visible with the Mie theory but is included through the dependency of the refraction index with the wavelength (Cauchy formula, Briot dispersion or equivalent).

The size of the haze particle: r = D/2

Fog particles have typically a radius of r=0.01um to r=1um. Thus, in the simulation made the dependency of the scattered field is simulated with three different particle sizes: 0.01; 0.1 and 1um. We will also observe the result electric field if we have fog composed with different particle size.

The complex index of refraction of the haze particle: m(λ)

As noted above, the complex index of refraction depends on the wavelength. In order to have good simulation results, it is necessary to have the most accurate measure for this parameter. To match better the reality, we will use the previous database [8] defined by the International Association for the Properties of Water and Steam which has been tested for a wavelength range up to 1900nm [9]. In their formulation, the real part, n, of the refractive index of water, m=n+ik, is expressed as:

$$\frac{n^2-1}{n^2+2}=\frac{\rho}{\rho^*}\left[a_0+a_1\frac{\rho}{\rho^*}+a_2\frac{T}{T_0}+a_3\frac{\lambda}{\lambda^*}\frac{T}{T^*}+a_4\left(\frac{\lambda}{\lambda^*}\right)^{-2}+\frac{a_5}{\left(\frac{\lambda}{\lambda^*}\right)^2-\lambda_{UV}^2}+\frac{a_6}{\left(\frac{\lambda}{\lambda^*}\right)^2-\lambda_{IR}^2}+a_7\frac{\rho}{\rho^*}\right] \quad (5)$$

With the following constants values:
a_0=0.244257733; a_1=9.74634476.10^{-3}; a_2=-3.73234996.10^{-3}; a_3=2.68678472.10^{-4}; a_4=1.58920570.10^{-3}; a_5=2.45934259.10^{-3}; a_6=0.900704920; a_7 = -1.66626219.10^{-2}; λ_{UV} = 0.2292020; λ_{IR}=5.432 937

and the dimensionless variables:

- temperature: T/T* (where T*=273.15 K)
- density: ρ/ρ* (where ρ*=1000 kg.m^{-3})
- wavelength: λ/ λ* (where λ*= 0.589 μm)

The problem of this formulation is that it does not provide the imaginary part of the refractive index of water (usually estimated as 0 in visible range) which could be crucial for scattering understanding.
For this reason, in addition to this database [8] used to determine the real coefficient of the refractive index, another one [10] was employed for the imaginary coefficient of water determination.

The electric field polarization.

The light coming directly from the sun is un-polarized. In other world, it is combination of arbitrary polarized light with arbitrary phase (stochastic distribution of polarization). To simulate with the program the effect of this light, a Monte-Carlo simulation was used: the program will generate hundreds of electric field with completely arbitrary incident polarized light and the scattering wave resulting of all those contributions is observed in far-field.

3.1.2 Simulation results

As discussed previously (see Eq. 4), the goal is to minimize the airlight component $I_{scat\,[particles]}$ relatively to the signal of interest I_{object}. Using the model implemented and the assumption detailed in Appendix B- Mie scattering, the following important simulation results on $I_{scat\,[particles]}$ can be observed (Figure 3 to 5):

3.1.2.1 Wavelength dependency of $I_{scat\,[particles]}$

The light scattered intensity ($I_{scat\,[particles]}$) depends on wavelength (Figure 3)

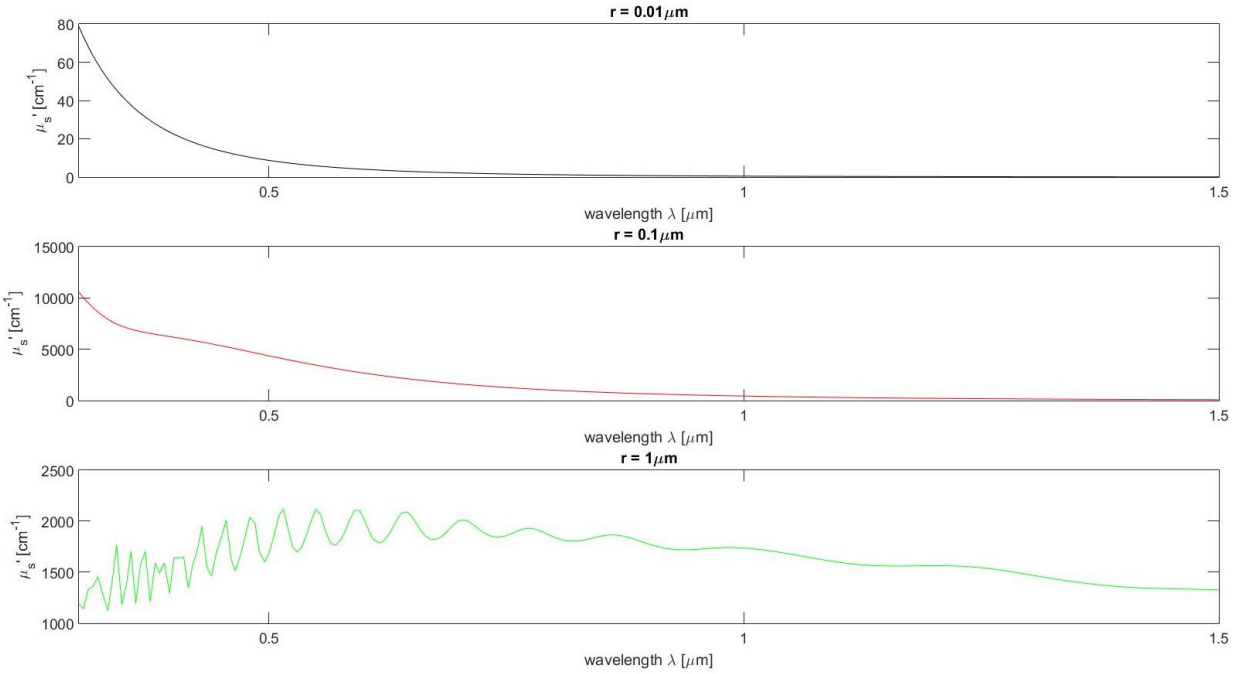

Figure 3: Evolution of the reduced scattering coefficient with the wavelength from visible to SWIR

The measure of the reduced scattering coefficient for the three particle size relative to the wavelength is plotted. This coefficient corresponds to the number of scatter event N observed during the propagation through a homogeneous scattering medium with a thickness d. In other word, if the reduced scattering coefficient is high, there is more haze effect.

For the smallest particles this factor decreases drastically with the wavelength [*Note that we can retrieve the factor* λ^{-4} *predicted in Rayleigh regime range*]. For example for a particle with r=0.1µm, using this simulation we can deduce at a wavelength of 1500nm (SWIR) compared to a wavelength of 500nm (visible) a reduction of the scattering events by 100. Thus, **haze effect will be GENERALLY less important for higher wavelength. Particularly, for the visible spectrum, the effect will be lower in the red than in the blue and less important in SWIR than in the visible spectrum**.

The last data plotted in this simulation (r=0.01µm) is really important. We can see that the behavior on this case is not the one expected in the Rayleigh regime. In this case, for specific wavelengths around 400nm (violet-blue light), scattering effects are expected to be less important than higher wavelength such as red (around 600nm) or even SWIR (around 1um).
Thus, we can conclude using this graphic that it is important to have a **multispectral acquisition system** (which is part of the solution proposed).

3.1.2.2 Polarization signatures of $I_{scat\,[particles]}$ *(Figure 4)*

If scattered light has specific polarization signature (due to the interaction between light and the aerosolized particle), there is no reason that the un-polarized sunlight directly reflected by the object will be the same. Thus, it is possible to minimize the airlight component $I_{scat\,[particles]}$ relatively to the signal of interest I_{object} by using this polarization information (see the *Multispectral polarization imaging solution* section for detailed on the dehazing method). Hereafter, we demonstrate experimentally this specific polarization signature of the light scattered.

a. The polarization signature of the scattered light ’s can be partially linear (Figure 4)

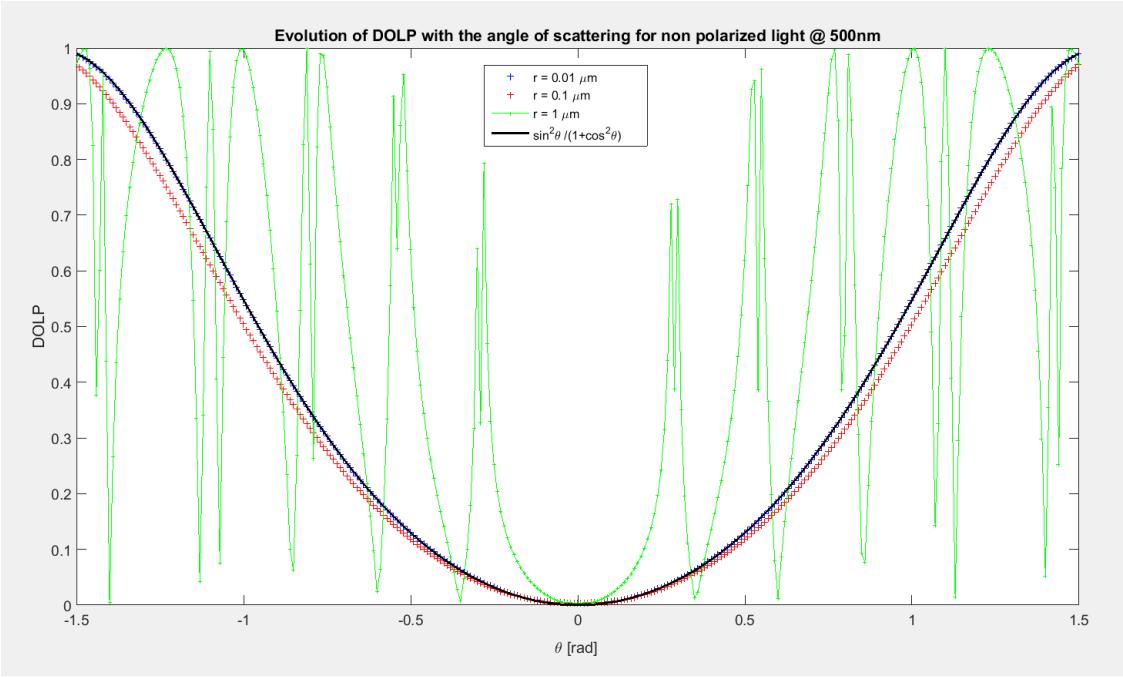

Figure 4: Evolution of the Degree Of Linear Polarization with the angle of scattering for non-polarized light at 500nm

The theoretical value for the Degree Of Linear Polarization (DOLP) using the Rayleigh model (black line) is compared to the one obtained with the Mie scattering model program described above. Three different radii sizes of particle r=0.01; 0.1; 1um and non-polarized light at λ=500nm are considered. The Rayleigh scattering model is a good approximation for small particle size compared to wavelength. Thus, we observe as the theory previse that the DOLP simulation result using Mie theory is similar to the result obtained with Rayleigh model for the smallest particle of 0.01um and differs from it for the biggest particle of 1um.
From this graph, we can conclude that the scattered light has a complex polarization signature that depends on different parameters such as the angle of scattering (angle between the initial and final directions of light propagating through the scattering particle) and the particle size. Thus, the polarization information can be used to differentiate the scattered photon from the ballistic photon directly reflected by the object.

We can conclude that it is important to have a **polarimetric acquisition system** (which is part of the solution proposed).

b. The polarization signature of the scattered light 's can be partially linear, circular or elliptical (Figure 5)

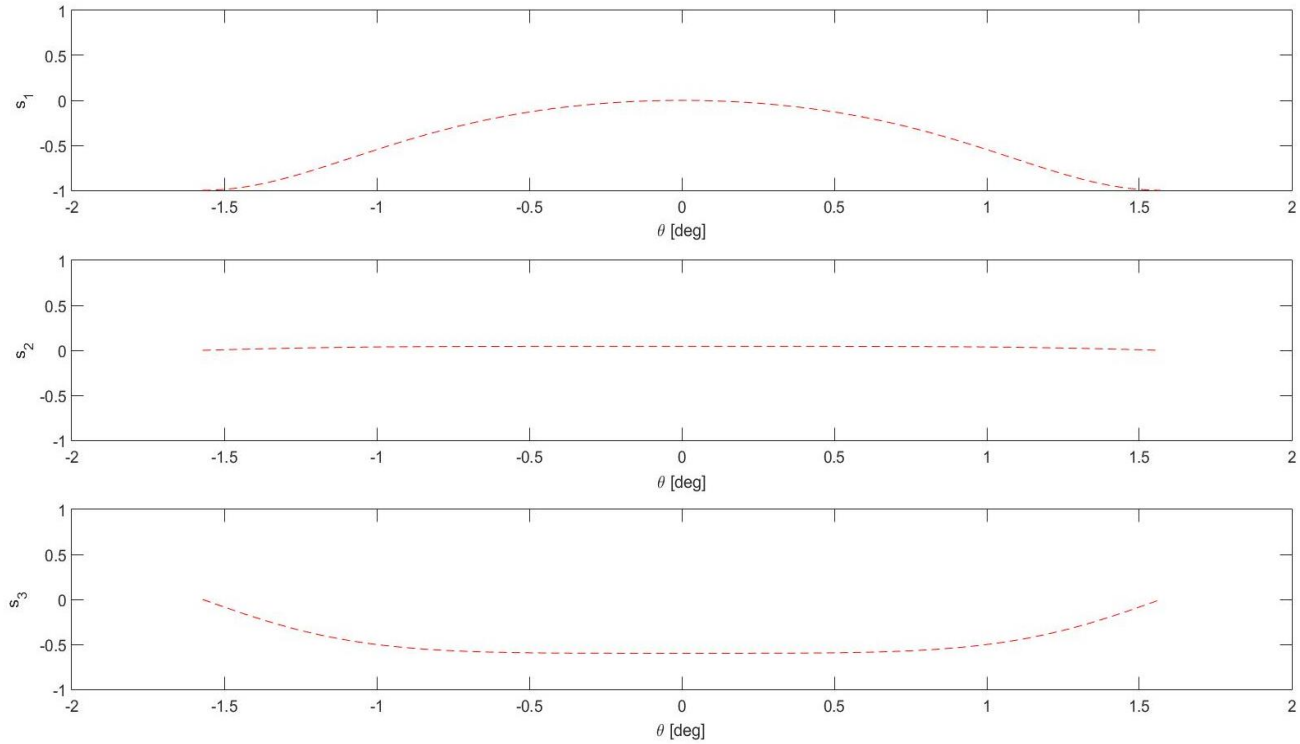

Figure 5: Evolution of the polarization with the angle of scattering (r=0.1µm)

The evolution of the normalized Stokes (s_1, s_2, s_3) vector depending on the angle of scattering is plotted for a particle with r= 0.1µm and an incident light wavelength λ =1500nm.

In figure 5, we can observe that the parameter s_1 fluctuates depending on the angle of scattering. Because the DOLP is expressed out of s_1 and s_2 (see appendix A), it also fluctuates (as it has been shown in figure 4).

It can also be noted that the presence of circularly polarized light (s_3), which was not predicted by the Rayleigh model. The circular polarization is useful not only because it provides additional data about the fog presence, but also because it is maximized when the linear components (s_1 and s_2) are at their minimum. In other words, information on the scattered light can be obtained for any scattering angle if polarization data is used properly.

We can conclude from this graph that it is important to have a **full Stokes polarimetric acquisition system**.

All the simulation runs and the results obtained (figure 3 to 5) lead to an acquisition system based on a **multispectral polarization imaging system**. The next section will detail this solution.

3.2 Multispectral polarization imaging solution

The multispectral polarization imaging solution proposed is a complete dehazing method based on three consecutive steps (see figure 6) that will take advantages of the information discussed in the previous section:

- Two acquisition steps (a spectral selection and a polarization modulation) in order to acquire the image with as few haze effects as possible.
- One post processing step on the image in order to complete image dehazing

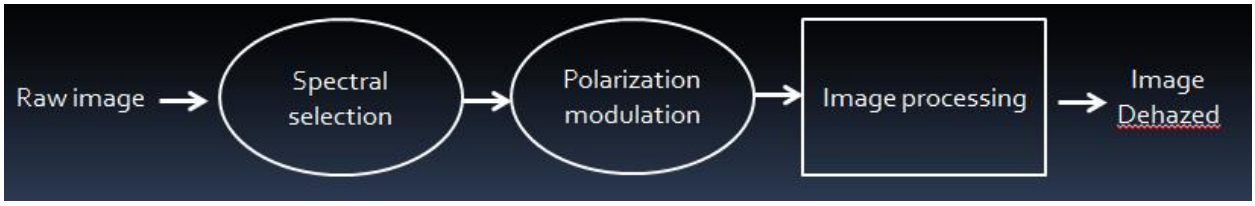

Figure 6: Basic architecture of the multispectral polarization imaging solution

3.2.1 First step: Spectral selection [acquisition]

As it has been pointed out during the simulation, the scattering effect depends highly on the wavelength considered (chromaticity dependency).

For this reason, in order to minimize haze effect, a spectral selection is used. This technique consists in observing the same scene with various spectral filters and selects the filter for the image acquisition where the haze effect is less present ($I_{scat\ [particles]}$ minimized) and the signal of interest is the strongest (I_{object} maximized).

In practice, this was done in the experiments during this Phase I effort by tuning the light source or by acquiring the same scene while changing manually the spectral filter in front of the camera or using the SWIR instead of the visible spectrum camera (on the field experiments).

In order to determine which were the images with less haze effects, various methods were explored which will be detailed on the results sections.

3.2.2 Second step: Polarization modulation [acquisition]

The light scattered by haze particles can present strong and very specific polarization signature.

In most cases the object observed does not feature the same polarization signature. Therefore, polarization imaging capabilities can be a very efficient tool to isolate and reject the light contribution due uniquely to the haze particles. Isolating that part is the first step to then attenuate it, and in some cases completely remove the blurring effect on the image.

But in order to do so, it is necessary to know precisely the polarization properties of the light reflected by the object directly toward the camera. The general assumption made is that **light**

directly reflected by the object is not polarized. This approximation is valid for objects with diffusive surface. It is mainly not valid for objects featuring specular, highly reflective surfaces. However, the more scattering particles are present, the lower the portion of light coming directly from the object becomes compare to airlight scattered by the obscurant.

It has been shown that **for an object far enough** [10] ($\beta z > 0.2$ with β coefficient of extinction due to scattering and absorption and z the distance between observer and object), **this general assumption becomes valid, even for specular surfaces** (see figure 26 for experimental validation). In other words, in presence of obscurant, the light reflected by an object far enough can be considered un-polarized.

The dehazing method becomes easy to understand by looking back at Equation (4). This equation can be rewritten:

$$I_{detect} = I_{scat\,[object]} + I^{\,pol}_{scat\,[particles]} + I^{\,unpol}_{scat\,[particles]} \quad (6)$$

The light detected is the superimposition of:

- $I_{scat\,[object]}$, unpolarized. This is what we need to isolate.
- $I_{scat\,[particles]}$, partially polarized. This is the contribution due to the obscurant particles, which need to be minimized.
  It is decomposed as $I^{\,pol}_{scat\,[particles]}$ and $I^{\,unpol}_{scat\,[particles]}$ wich are respectively the component of the scattered light completely and not polarized.

In order to minimize the second term of Equation 4, three different techniques based on polarization imaging were explored during this Phase I effort (see Appendix B-polarization modulation for details):

3.2.2.1 Using a "linear polarizer"

The idea is to add a linear polarizer filter on the light's pathway, whose axis orientation is adjusted in order to cut part of the polarized light coming from the haze particles scattering.

Although attractive because of its simplicity, this technique only produces limited results. This is due to two reasons:

- Light scattered is only partially polarized
- The polarized part of the scattered light is not purely linearly polarized, except in rare configuration (see figure 4). Most times it is partially, elliptically polarized.

The consequence is that a linear polarizer cannot remove completely the contribution of scattered light.

3.2.2.2 Using the measured Degree Of Polarization

Since the assumption made is that the light coming from the target is un-polarized, one method consists of removing all the polarized part of the light. By using a polarization camera, we can extract the DOLP and thus separate the image into its totally polarized part and un-polarized part. The totally polarized part can be excluded to recover only the light coming from the target. Again, there is a limitation with this approach. This technique removes only the polarized component $I^{pol}_{scat\,[particles]}$ and not the non-polarized component $I^{unpol}_{scat\,[particles]}$ of the light scattered $I_{scat\,[particles]}$ (see Eq.6).

3.2.2.3 Using the extended Degree Of Polarization extracting technique

This technique is an extension of the previous method. It is based on three steps:

1- Measuring the polarized part of the scattered light: $I^{pol}_{scat\,[particles]}$

This can be done by using the technique described in the section above.

2- Measuring the ratio $I^{unpol}_{scat\,[particles]}/I^{pol}_{scat\,[particles]}$ ***on the scene***

The additional assumption made is that the scattering angles (the angle between the light source, the haze particle and the line of sight) and the nature of the particles are constant within the scene observed. As a consequence, the ratio between the un-polarized and polarized parts of the light scattered $[I^{unpol}_{scat\,[particles]}/I^{pol}_{scat\,[particles]}]$ by the obscurant remains constant as well. In other words, the only variations observed within the scene are due to the difference of fog density between the scene and the observer.

This ratio can be measured on a known point where only airlight is present (clear sky for example).

3- Remove completely $I_{scat\,[particles]}$ ***on each pixel of the scene***

$I^{pol}_{scat\,[particles]}$ has been measured via the measurement of the Degree Of Polarization (DOP) for each pixel of the scene.

The ratio $I^{unpol}_{scat\,[particles]}/I^{pol}_{scat\,[particles]}$ has also been estimated and is assumed to remain uniform across the image.

Therefore, $I^{unpol}_{scat\,[particles]}$ can be estimated for each pixel of the scene.

We now have estimated the two contributions of the total light scattered by the haze particles, its polarized and its un-polarized parts: $I_{scat\,[particles]} = I^{pol}_{scat\,[particles]} + I^{unpol}_{scat\,[particles]}$

3.2.3 Third step: Post processing techniques

Once images have been acquired at a specific wavelength(s) and polarization imaging techniques have been applied, the last step is to apply well-known image processing tools.

The model widely used for post-processing techniques to describe hazed images is [11-14]:

$$I_{detect}(x,y) = J(x,y)t(x,y) + V(x,y) \quad (7)$$

With $\mathbf{I_{detect}}$ the intensity detected by the camera, **J** the scene radiance, **t** the medium transmission, and $\boldsymbol{V(x,y) = A(1 - t(x,y))}$ the atmospheric veil where **A** is the global atmospheric light, and **(x, y)** is the pixels coordinates of the scene.

The problem with this model is that it is a dependent system of equation: there are three unknown parameters for only one equation (infinity of possible solutions). Thus, in order to solve this problem, some additional physical constraints need to be applied.

The main assumption used is to consider that the atmospheric veil (and consequently the transmission map) has no specific edges or textures.

So, in order to estimate the haze layer or atmospheric veil from the hazy image, a low pass filter is applied to the image. The equation system is composed of two independents equations with three independent unknown parameters:

$$\begin{aligned} I_{detect}(x,y) &= J(x,y)t(x,y) + V(x,y) \\ LowPass(I_{detect}(x,y)) &= V(x,y) \end{aligned} \quad (8)$$

Then, in order to fully solve the problem, the general technique involves determining the airlight parameter A by measuring it in area where it is perfectly known such as sky where

$$I_{detect}(x_{sky}, y_{sky}) = A \quad (9)$$

This way, the transmission map can be recovered and thus, the intensity of the dehazed image.

However the transmittance map recovered suffers from the strong assumptions made which are not perfectly verified on whole image or for all geometrical configurations of objects in the scene. Additional filters are generally used to smooth the obtained transmittance.

The basic principle is summarized in figure 7 (for more details please refer to Appendix B-Post-processing techniques).

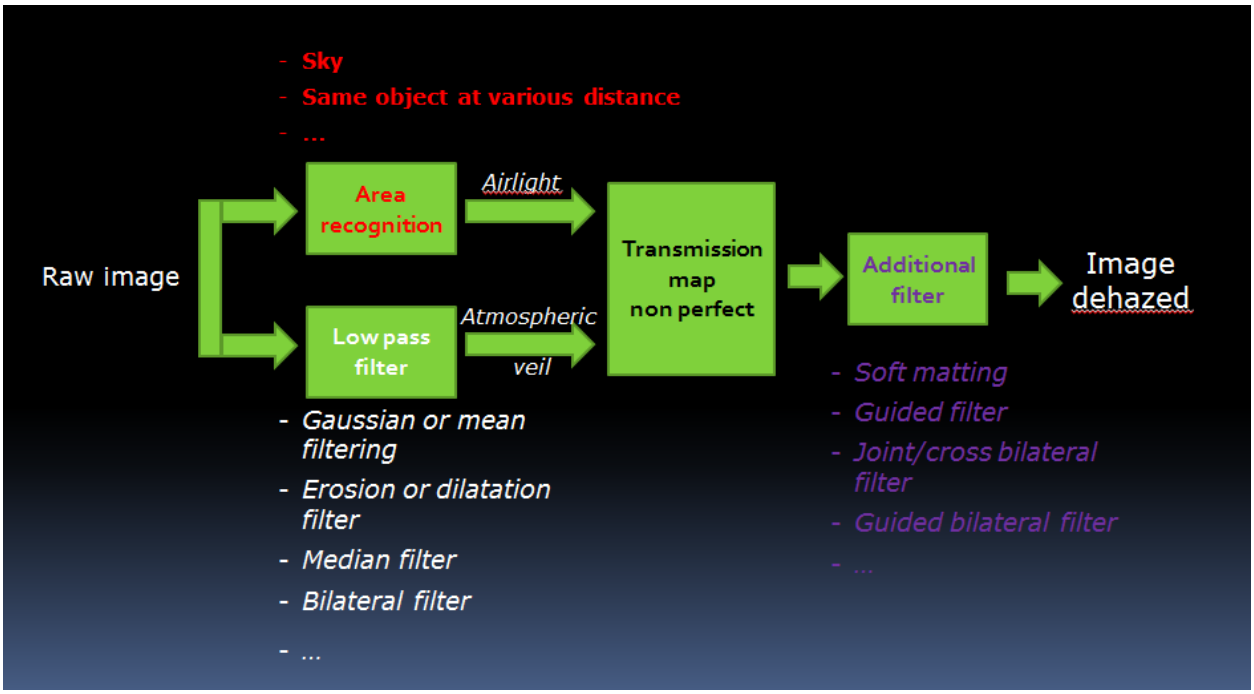

Figure 7: Basic architecture of post-processing techniques to recover an image dehazed from a raw image

This first study was limited on the case of dark channel prior (DCP) technique [14] (for more details please refer to appendix-Post-processing techniques) which presents the combination of relatively good efficiency and computational speed [15].

3.3 The Testing environment

In order to evaluate and validate the dehazing system, two completely different environments have been tested: a fully controlled lab-setup (in order to validate the methodology and the concept) and a non-controlled environment (in order to validate the performances in real condition).

3.3.1 Fully controlled lab-setup

For the laboratory setup, two main constraints have been followed: 1- The laboratory setup should closely mimic the behavior of fog in natural condition, 2- it is necessary to have a complete control of the experimental setup.

The fully controlled experimental testing setup is composed of a transparent tank, a scattering medium, an illumination, the Salsa Full Stokes polarimetric camera and a target (see Figure 8).

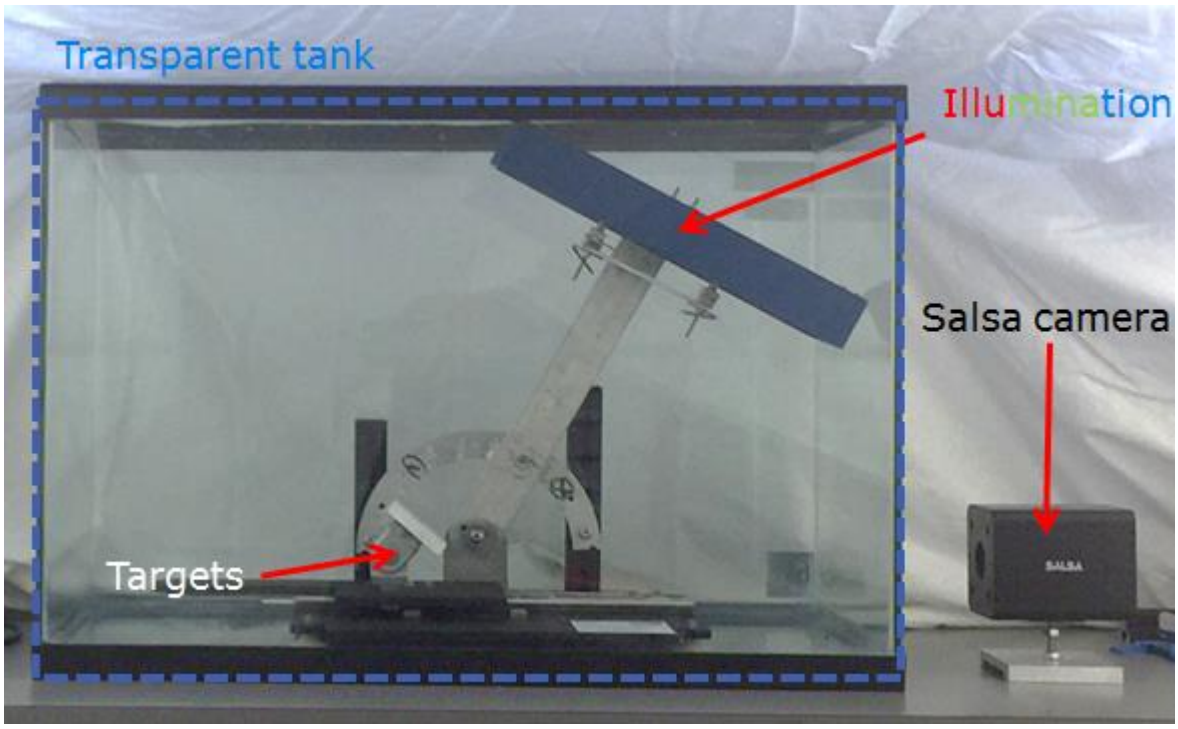

Figure 8: Experimental testing setup

The transparent tank

The principle of having a transparent tank is to be able to control the quantity of scattering particles. To do so at low price, the solution adopted was to use an object specially designed for it: an aquarium. There are mainly two different types of aquarium enclosure: acrylic and glass. Acrylic element (such as CD case [16]) have strong polarization signature. Thus, it is not a good enclosure to test the polarization modulation dehazing method developed. For this reason, the transparent tank used is a glass aquarium.

The scattering medium

In order to mimic fog behavior, many different techniques can be employed: fog machine, milk+water, fog effect glass filter…

A fog machine presents the advantage to look like the fog that could appear in outdoor environment. But using directly a fog machine can be challenging at this validation step since it is not proven that a manmade fog will have the same behavior as fog in natural condition in every aspect. Many factors are also not under control such as the size of the particles, the exact composition, the distribution in space, the concentration…

On the other hand, a fog effect glass filter is exactly under control but has no degree of freedom (for example no modification of "fog" concentration possible).

In haze, the typical size of the particles is 10-1000nm. The whole milk usually contains approximatively 2.7% of casein (~ 0.04-0.3 µm) and 3.4% of fat globule (1-10 µm) [17, 18]. Due to their size and index of refraction, milk + water solution is usually used to mimic the effects of

fog scattering. This technique was used here to validate our system since it is completely controllable and it provides similar results as the one encountered in fog.

To simplify the problem and consider only one kind of particle in our experiment, low fat milk [19, 20] (where only casein is present) will be used in the result presented. Three different volume percentage of milk were used 0.013, 0.009 and 0.007%.

Illumination

To mimic the sunlight, a non-polarized white light illumination was used. The illumination is composed of a grid of diodes (enclosed in a waterproof case) and a diffuser (see figure 9).

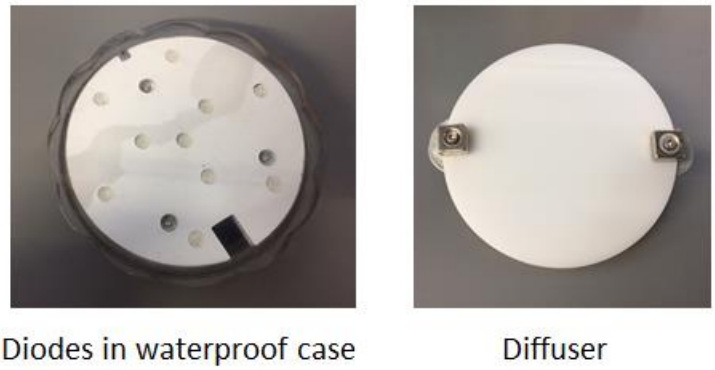

Figure 9: Illumination

The illumination can provide white light or bandpass red, green or blue light. The waterproof case will allow in the experiment to submerge the light during the water experiments [This way, there is no partial polarization induce by light transmitted after an air-water interface that would create artefact during polarization modulation method].The light Diffuser is a diffuser film designed to break up and distribute light evenly.
The illumination is placed on a rotating stage (figure 10) so the angle defined by the illumination, the object and the camera can be adjusted without modifying the target-camera distance.

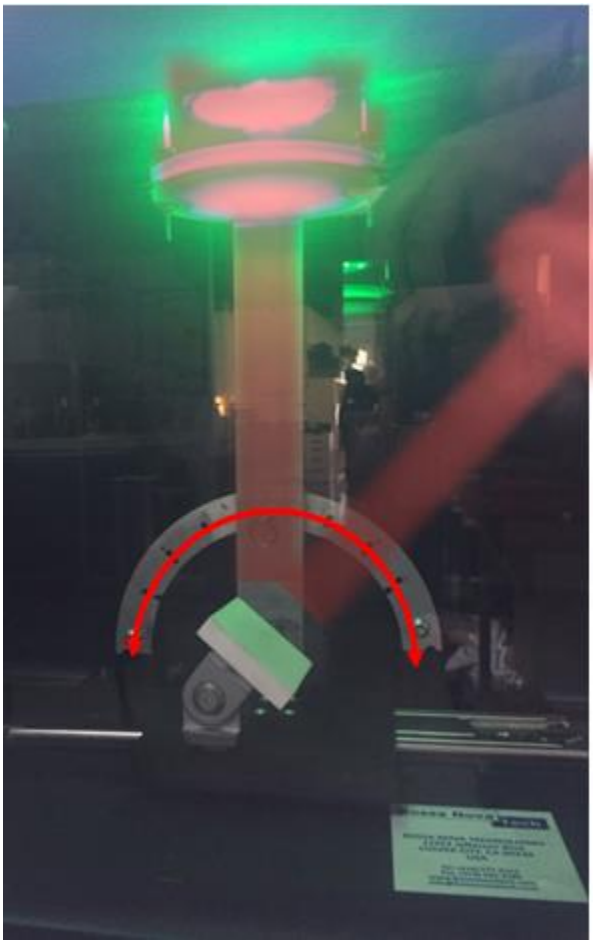

Figure 10: Rotation stage for the illumination. Some of the configurations available for the illumination are presented in red shape.

Full Stokes polarization imaging camera (visible spectrum)

The Salsa Full Stokes camera is our polarization camera (figure 11).

Figure 11: Salsa Full Stokes visible camera

The objective lens used in the experiments presented has a focal length of 25mm. Bandpass red, green and blue filters were used during our laboratory experiments and laser line filters at 400,

450, 500, 600, 650nm with FWHM=10nm where used for outdoors experiments. For each of those filters, the camera has been calibrated by running a process during which several hundred known polarization states are generated and measured by the SALSA camera. It means that for each wavelength used, we have determined the calibration matrix *C* which links the 4 raw frame images acquired successively (I_0, I_1, I_2, I_3) with the 4 Stokes parameters (S_0, S_1, S_2, S_3) using the data reduction matrix technique [16, 21-23].

$$\vec{S} = C * \vec{I}$$

The target(s)

Light reflected by objects can be polarized or not depending on its surface [24]. However, as we have discussed in *Multispectral polarization imaging solution-polarization modulation* section, when the object is far enough, the light emanating from scene objects has insignificant polarization contribution to the measured polarization.

To test and verify this hypothesis, two different objects were used during the laboratory experiments (see figure 12):

- A square spectralon (from labsphere): diffusive surface.
- A toy car: specular surface.

Figure 12: Targets

The configuration

Two different configurations have been considered (figure 13).

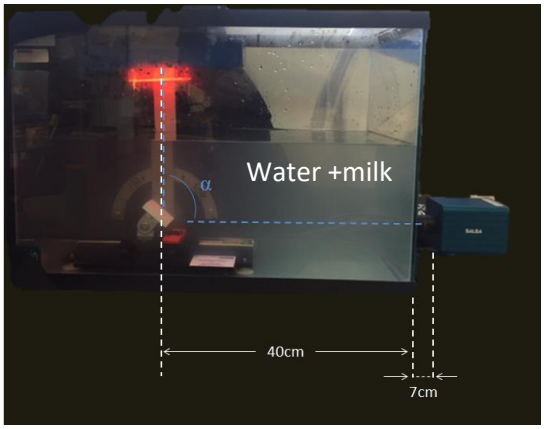

Configuration 1

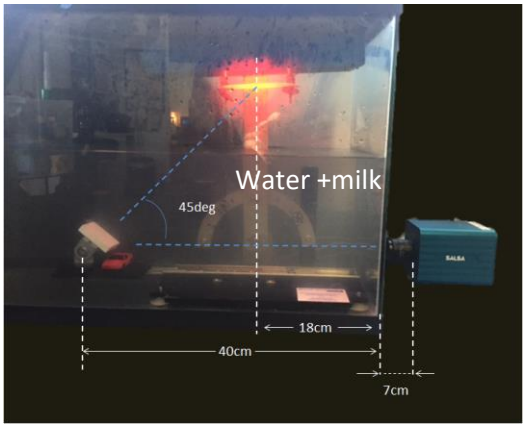

Configuration 2

Figure 13: The two different configurations used during the experiments. In configuration 1, the angle α can be adjusted from 40 to 90deg. In configuration 2, the angle is fixed.

In the first configuration, the angle α defined by the illumination, the target and the camera can be adjusted. The main component of airlight is induced by forward scattering in small particles.

In the second configuration, the angle defined by the illumination, the target and the camera is fixed to 45deg. The component of airlight is induced by forward and backward scattering in small particles.

This two different configurations and the different concentration of milk allows mimicking natural behavior of fog in various conditions.

3.3.2 Non-controlled environment

For this setup, we considered outdoor environment. Two main guidelines have been followed to determine the scene to observe: 1- The haze observed needed to be similar as the one that can be observed on shipboard environment (therefore, we select a coastal scene), 2- The scene should be highly textured in order to quantify dehazing improvement (thus, we select a scene where lots of buildings are present).

The scene selected was the shore of Santa Monica, CA. It was observed from Manhattan Beach, CA (figure 14). The scene was observed using the Salsa Full Stokes polarization camera described above and a SWIR non-polarimetric camera.

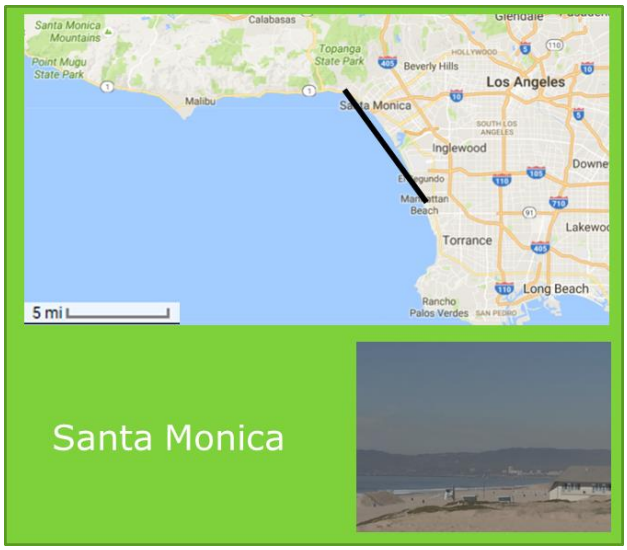

Figure 14: Image of the scene observed for on field experiments (Santa Monica) and map of the distance between the observation point (Manhattan Beach) and the scene (Santa Monica)

a. SWIR camera

The SWIR camera sensor used was an InGaAs sensor which has the best efficiency for this bandpass [1-3um] (see figure 15)

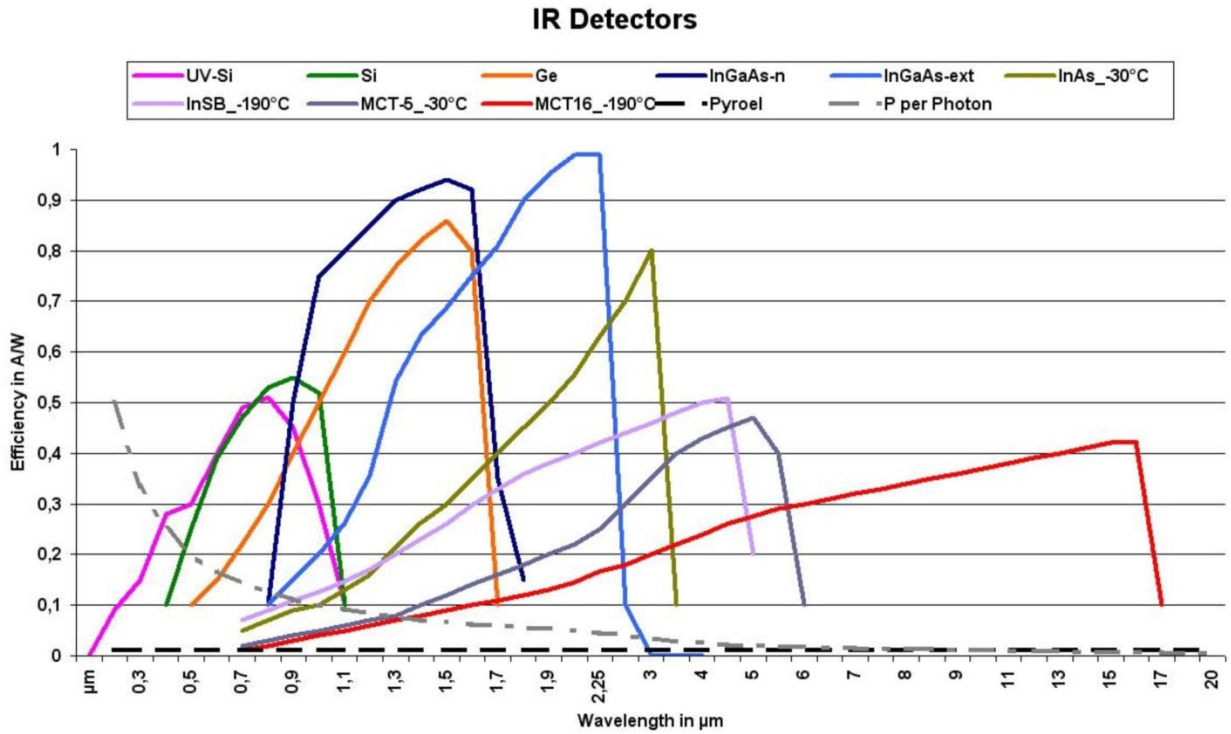

Figure15: Efficiency of some solid state detector depending on wavelength.

The choice of the sensor itself has been made to maximize the signal to noise ratio and have a high frame rate with high resolution SWIR camera. The main characteristics of the SWIR camera used are presented in Table 1.

Sensor	SWIR camera
Resolution (pix)	636 × 508
Wavelength range	900 to 1700nm
Cell size (um)	25 x 25
Temporal dark noise	400e-
Dynamic range	73dB
Quantum efficiency @ 1300	73%
Max Frame rate	100 fps

Table 1: Main characteristics of the SWIR camera

We can note that the camera sensor used has greater than 99.5% operating pixels. This is an excellent ratio for InGaAs sensors.

b. Evaluation techniques

Two types of techniques can be implemented in order to evaluate dehazing performances: qualitative and quantitative methods (see Appendix A-Performance metrics for more details).

Most of qualitative methods are made by using human perception [25]. The advantage of this method is that it is not this way necessary to have a strong knowledge of the dehazed scene to determine the dehazing method efficiency. However, this technique has many limitations:
- Quality depends on the observer perception
- Dehazing method efficient for human perception will not be automatically the best one for automatic detection (like the best sensor in SWIR is not the best for visible)
- Autonomous technique cannot be done with this technique
- There is no discrete scale on the dehazing efficiency (a dehazing technique will be good or bad)

On the contrary, quantitative methods could have all this advantages. The main limitation of those methods is that they generally require information on the dehazed scene. This limitation makes most of quantitative less useful for real-time identification. However, some quantitative techniques do not need this dehazed input. Some of those techniques mentioned in Appendix A-Performance metrics and on the results sections can be interesting especially for a fog algorithm assessment and/or a dehazing quality measurement.

3.4 Results in a controlled environment

3.4.1 Spectral selection

In this section we will present some of the results obtained with the polarimetric camera operating in the visible spectrum, using the laboratory system (presented in *3.3.1 Fully controlled labsetup*). They are divided following the same scheme as the dehazing method presented in figure 6: Spectral selection, polarization modulation and image processing.

The diffusive and specular targets are observed under three different illuminations (red, green and blue) and three different concentration of scattered particle (figure 16).

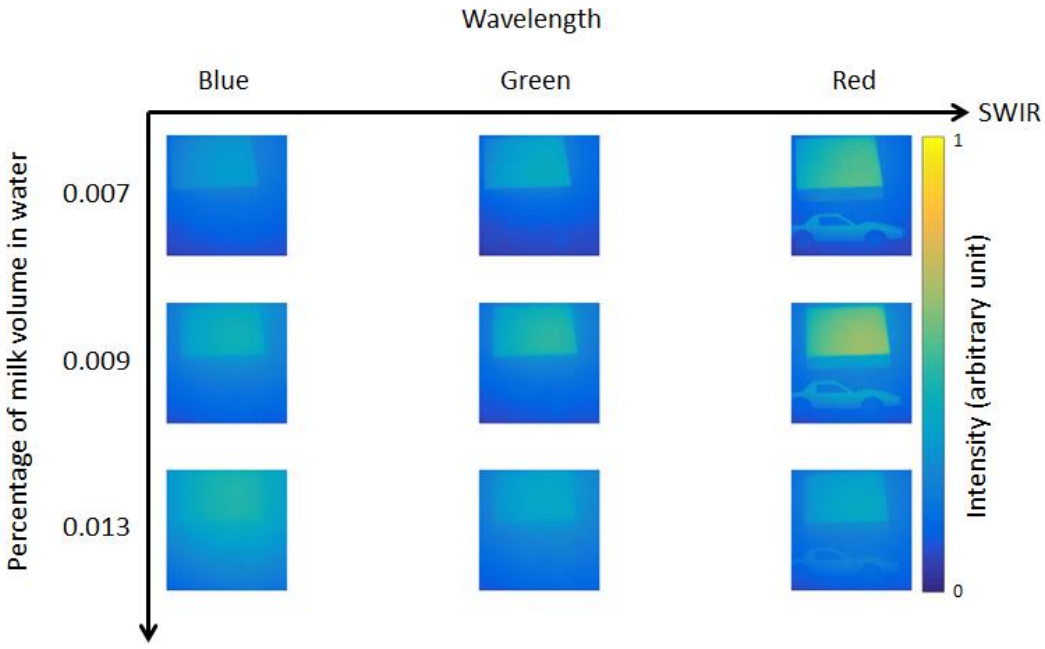

Figure 16: Evolution of the visibility depending on the wavelength and the milk volume percentage in the configuration 2 (see figure 13)

In this figure, we can clearly note the advantage of using a spectral selection during the acquisition. It can be observed that the best configuration to see clearly the object is obtained for a low concentration of milk (as expected) and a higher wavelength (red).

The size of the scattering particles in the experiments ranging from 0.04 to 0.3µm, those results are in agreement with the result obtained using the Mie theory (see figure 3).

3.4.2 Polarization modulation

Two techniques are presented here: the linear polarizer technique and the extended degree of polarization extraction technique (see the *Multispectral polarization imaging solution* section for detailed).

3.4.2.1 Using a linear polarizer

The light intensity image obtained through a perfect linear polarizer which axis lies at an angle ϕ with respect to a horizontal plane is given by the relation:

$$S_0^{Polar}(x,y,\lambda) = \frac{\left(S_0^{detect}(x,y,\lambda) + cos(2\phi)\, S_1^{detect}(x,y,\lambda) + sin(2\phi)\, S_2^{detect}(x,y,\lambda)\right)}{2} \quad (10)$$

The SALSA polarization camera actually measures all the Stokes parameters ($S_{0,1,2,3}^{detect}$), therefore it is possible to simulate the effect a perfect linear polarizer would have had on the image acquired.

It is assumed that only airlight contributes to the polarization signature. The light coming from the target is un-polarized. The goal is to minimize the contribution of the polarized light. Therefore, we can search for the polarizer's orientation angle ϕ that will give the minimum intensity $S_{0,\mathrm{Polar}}$ and it will correspond to the most efficient dehazing.

Figure 17, shows the evolution of the light intensity averaged over a Region Of Interest (drawn on the diffusive target) that would be measured after a linear polarizer for various angle ϕ. Three different position of the light source were considered (angle α).

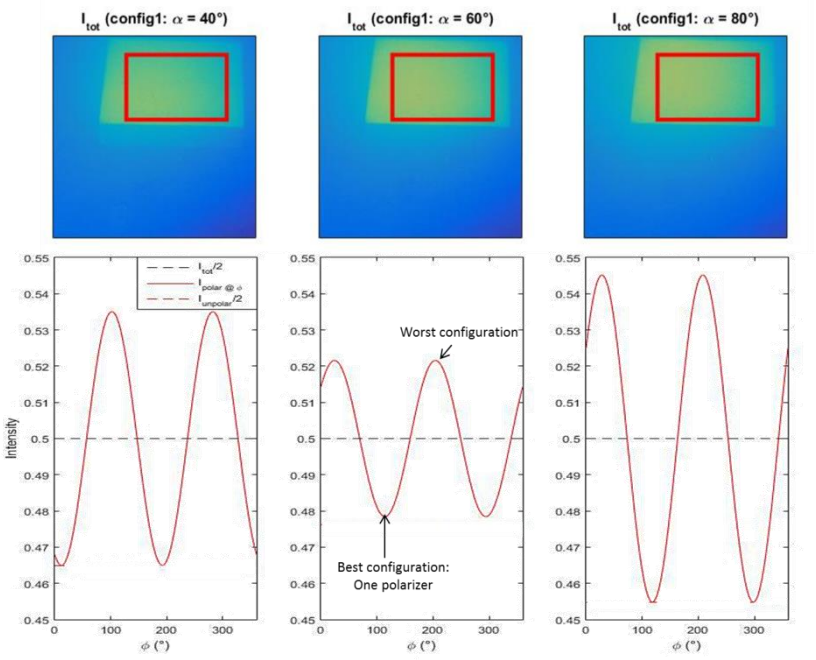

Figure 17: On top: Image of the diffusive target obtained with blue illumination and 0.007% of milk volume concentration. The red rectangle represents the ROI used to measure the intensities values. Bottom: Evolution of intensities in the ROI that would be obtained if a polarizer at an angle ϕ was placed in front of a simple camera (red line) compared to the total half-intensity acquired with a simple camera (black dashed line).

We can make the following observations and comments:

- We do see a modulation of the light intensity when changing the polarizer's orientation
- The amplitude of the variation is up to 5%
- The light intensity minimums are obtained for different polarizer's orientations ϕ in each case.

Consequently, this method could attenuate the contribution of the haze particles by up to 5% and requires **an adaptive polarization configuration that would search for the best axis orientation in each case.** Having an actual, mechanical rotating polarizer is simply unrealistic for real-time imaging. However, a Full Stokes polarization imaging system combined with adaptive software that automatically finds an optimal combination of linear polarization to enhance the image would be the best solution for dehazing using this method.

3.4.2.2 Using extended degree of polarization extraction technique

To demonstrate the dehazing efficiency of this method, an image of the diffusive target was acquired when no scattering medium was present (clear atmosphere) and then again when the scattering particles medium was added into the aquarium.

Then, two of the polarization dehazing techniques presented earlier were applied on the image. We tried to determine how the contrast between the target's edges and the background evolved.

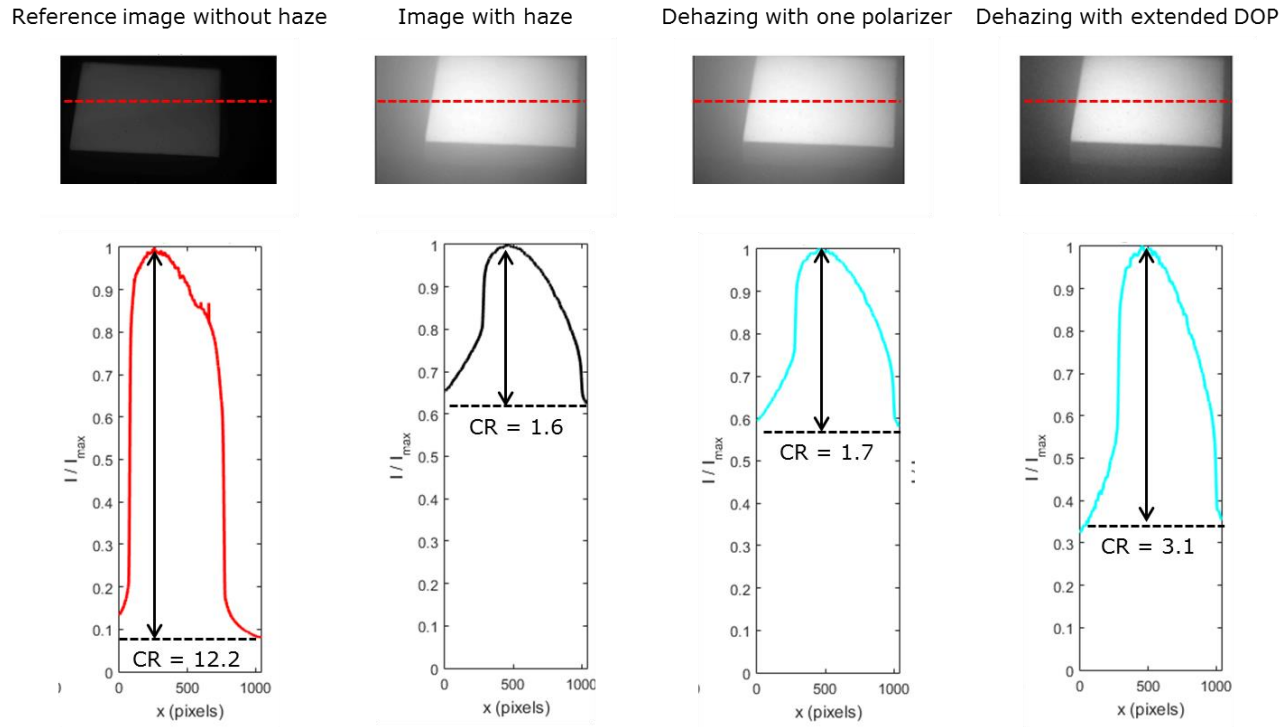

Figure 18: Top: Evolution of intensities detected before and after polarization dehazing processing for a 0.007% milk volume concentration and green illumination in configuration 2 (see figure 13). The first image serves as a reference when there is no scattering particle present. Bottom: Evolution of the normalized intensities values along the red dashed lines on the top of the figure.

On the top row of Figure 18, we can observe **qualitatively** that the image dehazed with extended DOP extraction technique provide a much better contrast than the image with haze or the image dehazed with one polarizer.

In order to evaluate **quantitatively** the improvement we measure the evolution of the intensity along a line on the image crossing areas where the target is and where there is no target. This allows to define a contrast ratio between the highest intensity observed (measured on the target) and the lowest one (measured where there is no target). We measure the same contrast ratio on the image without haze in order to have the reference of the image that should be obtained with complete dehazing. In this experiment, the presence of haze reduces the contrast ratio by a factor 8 (figure 18, between images 1 and 2).

Using the linear polarizer technique presented earlier does not increase drastically the contrast ratio (Figure 18, between images 2 and 3). The extended DOP extraction technique gives much better results (Figure 18, between images 3 and 4): the contrast ratio is improved and no noise is added to the image. The contrast ratio between the image dehazed and the regular image is increased by a factor 2 on this experiment.

3.4.2.3 Image processing

On figure 19, the results of the application of the DCP (dark channel prior) technique (for more details please refer to Appendix B-Post-processing techniques) on the image dehazed with extended DOP is provided.

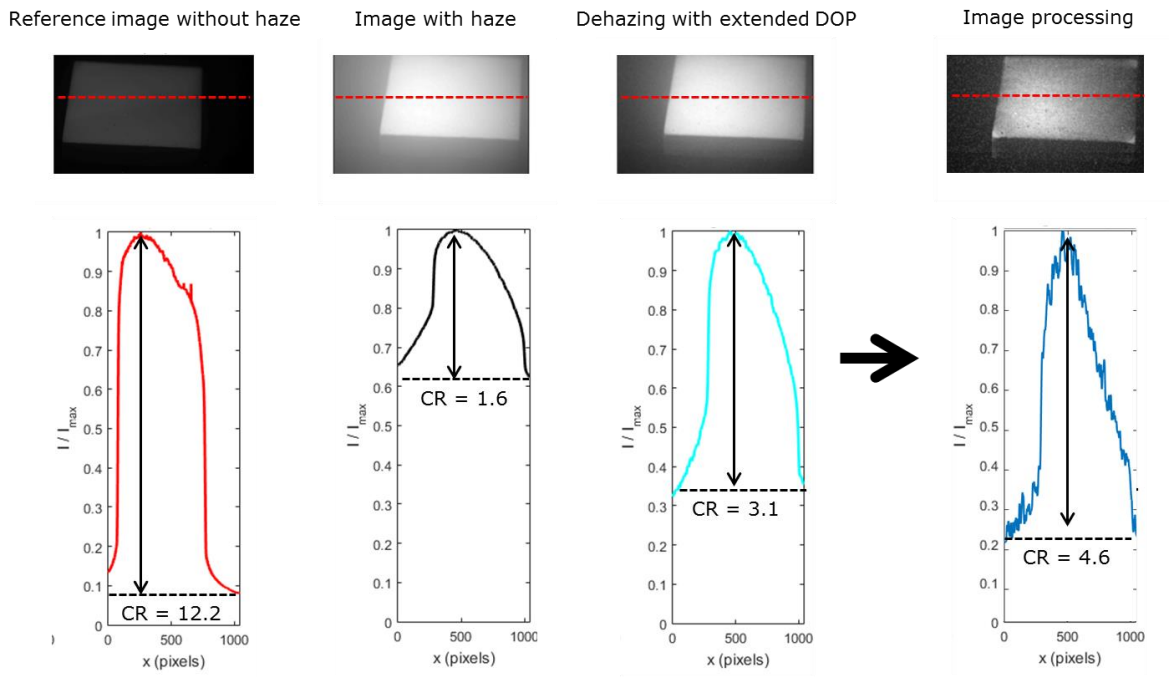

Figure 19: Evaluation of the image processing dehazing efficiency on the image dehazed with extended DOP. Same experimental conditions as figure 18

Using this post-processing technique allows to increase the contrast ratio by a factor 3 compared to the image with haze on this experiment. However, we can note that even if this image have

higher contrast ratio than the image dehazed with extended DOP technique it is noisier than expected (compared to the reference image without haze).

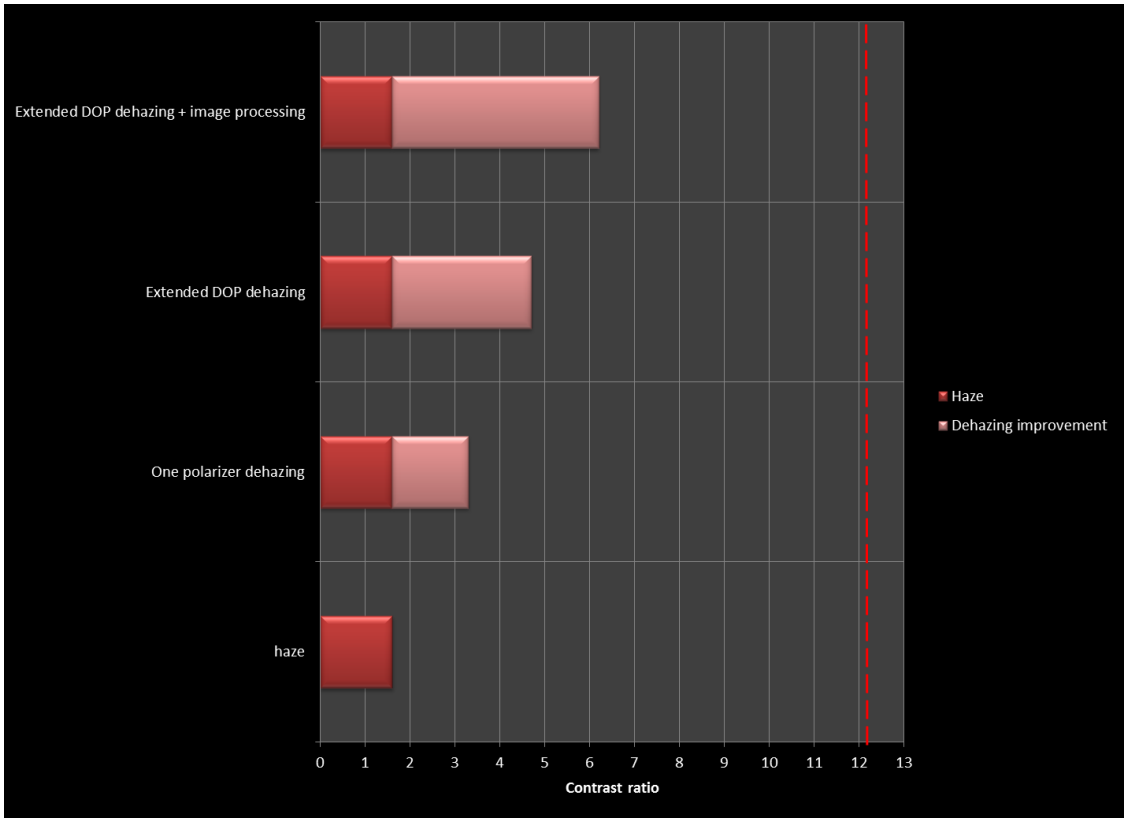

Figure 20: Contrast ratio enhancement on the results provides in figure 18 and figure 19. The dash line represents the contrast ratio measured without haze.

From this result (summarize in figure 20), we can conclude on the necessity of having a fog assessment method (one of which is presented in the next section) based on quantitative evaluation to determine when it is judicious to use each technique.

3.5 Results in a non-controlled environment

In this section we report on the results obtained during the outdoor experiments described in the *testing environment* section. We used the polarimetric imaging system for the visible wavelengths as well as a non-polarimetric SWIR camera.

3.5.1 1st Step: Spectral selection

The same static scene was observed through different spectral filter using the polarimetric camera. The results are display in figure 21 a).

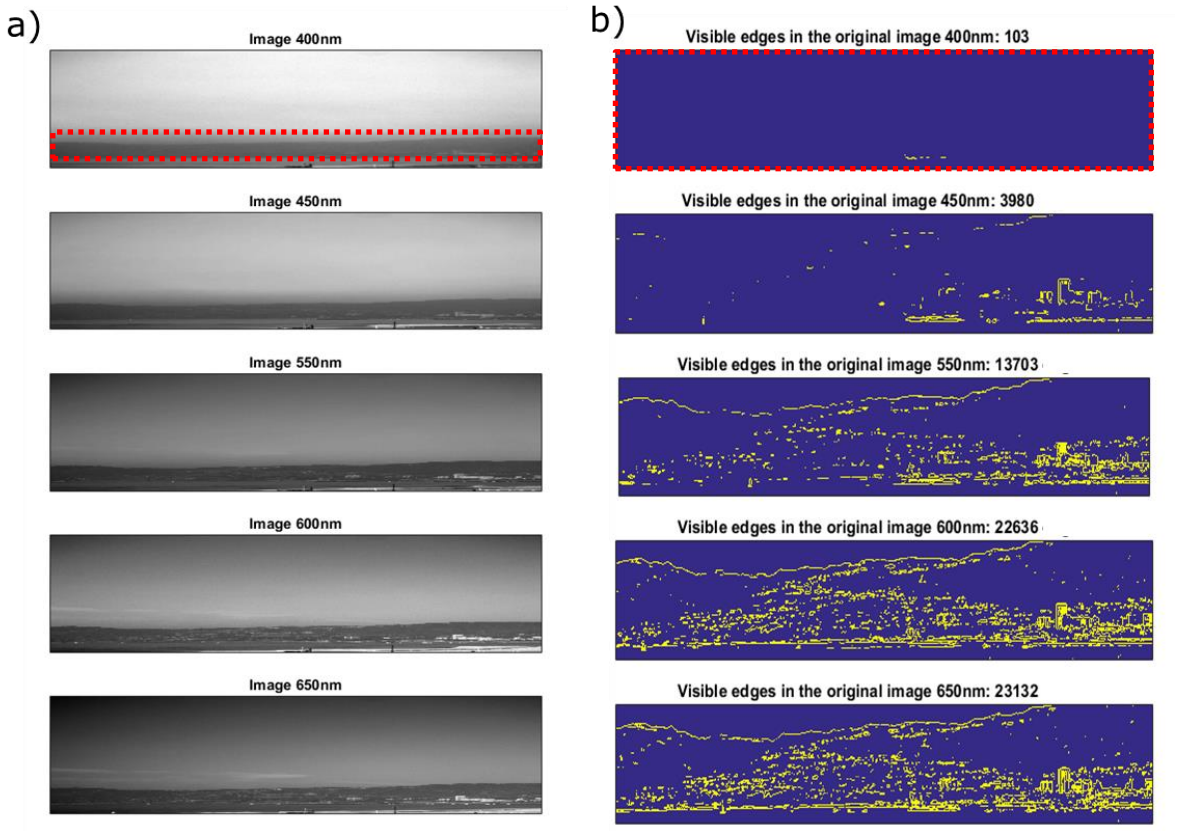

Figure 21: a) Intensity of the same scene under the same climatic conditions but observed through different spectral filter and b) Image and number of edges visible on the ROI (red rectangle) in the intensity image using gradient ratioing method [26].

It can be observed in this experience (figure 21.a) that the haze effect is less important in higher wavelength (650nm) than in low wavelength (400nm).

In order to evaluate this effect without scene knowledge, we used an edges detector tool on the images [26] (figure 20.b). When haze is present, the contrast on the image gets reduced. Thus, if the image is segmented (following the definition of the meteorological visibility distance proposed by CIE {the International Commission on Illumination} in 1987) the number of edges detected gives a good metric to evaluate the haze effect. **High number of visible edge** means more contrast so, **less haze effect**. Quantitatively, we can observe that spectral selection **increases by 231 times** the number of edge visible (figure 22).

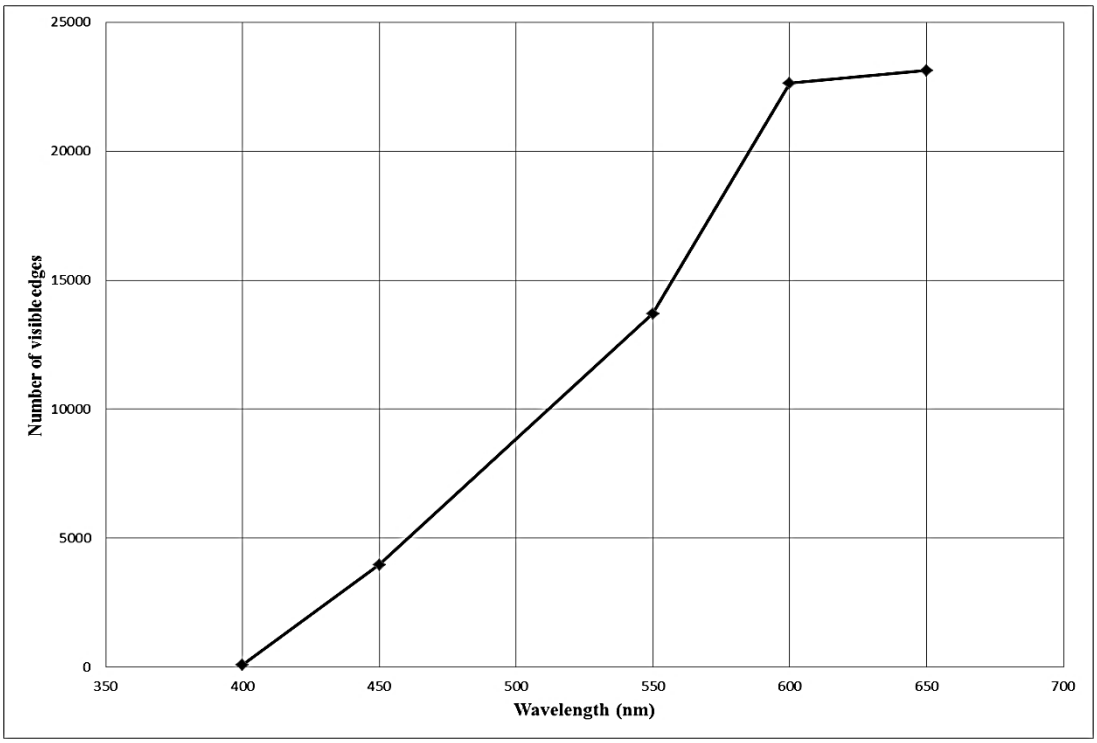

Figure 22: Evolution of the number of visible edges detected on the experiment displays in figure 21.

Because in this experiment the haze effect is less important for higher wavelengths in the visible range, we could expect good results with the SWIR camera.

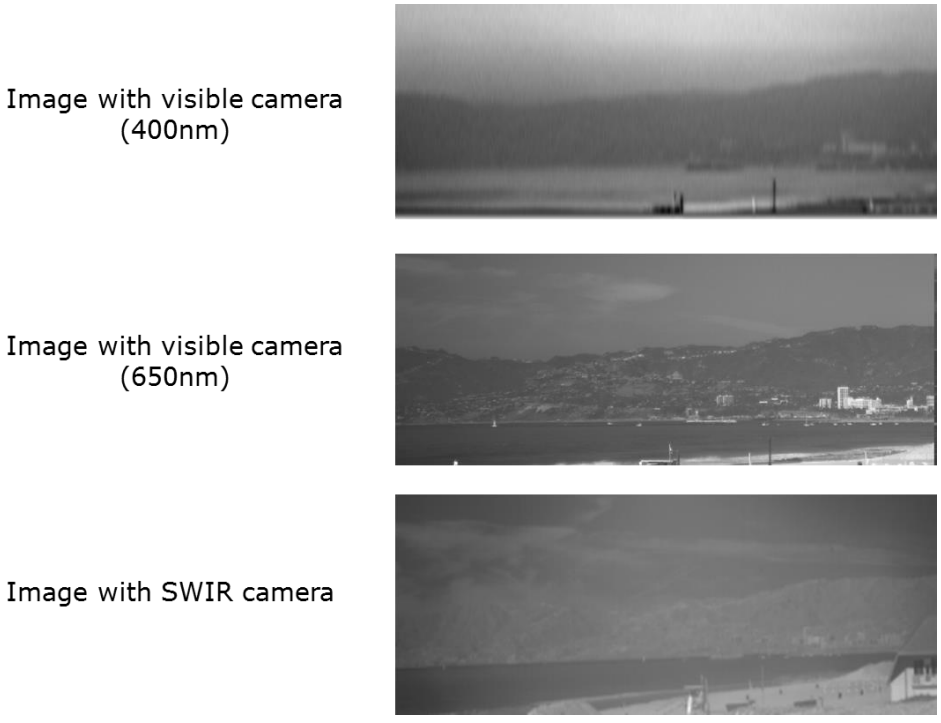

Figure 23: a) Intensity of the same scene under the same climatic conditions but observed the visible camera at 400nm and 650nm and with the SWIR camera

Figure 23 represents the same scene observed with the visible camera equipped with spectral filters centered at 400nm (blue), 650nm (red) and with the SWIR camera. If we focus on the mountain edges, we can notice that the image obtained with the SWIR in this fog condition is better that the one obtain with the visible camera at 400nm but clearly worse than the one obtained with the visible camera and a filter centered at 650nm.

However, it should be emphasized that the SWIR camera did not operate with a specific wavelength. The images acquired are cumulating the contributions of the entire SWIR, which could have destructive effects on the image.

For that purpose, we have dedicated Phase I.B effort to study the best configuration possible within the SWIR and the NIR spectral bandwidths.

3.5.2 2nd Step: Polarization modulation

On the best image obtained with the spectral selection (visible camera at 650nm), we applied the polarization imaging techniques described above (see *Appendix B-polarization modulation* for details). The result obtained is presented in figure 24.

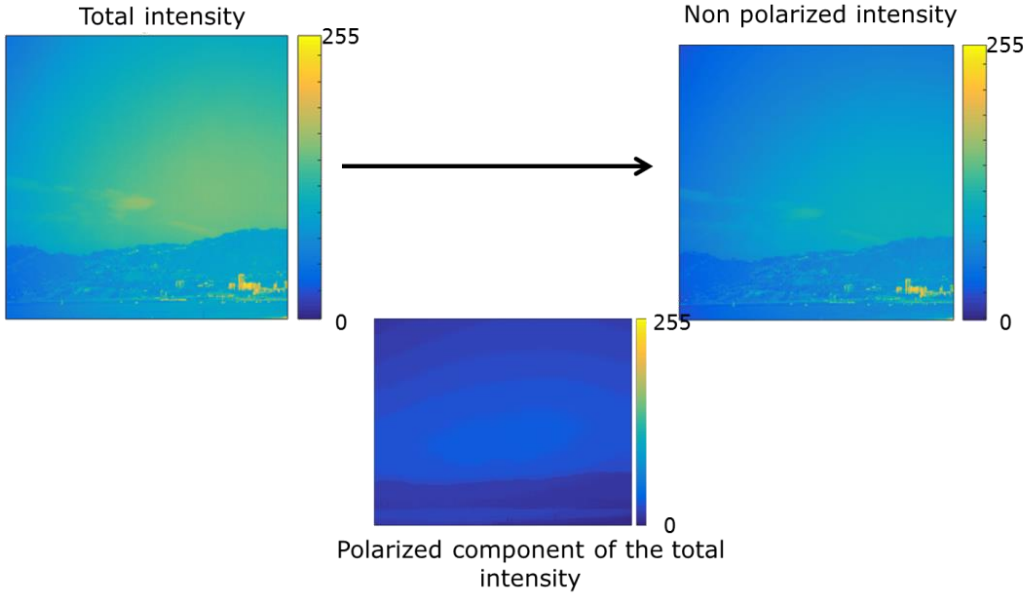

Figure 24: Image obtained at 650nm (figure 20) dehazed by using the polarization imaging technique. The image dehazed corresponds to the non-polarized intensity.

We can note that this method further increases the quality of the image. We performed the same evaluation technique based on the visible edges detected. The number of edge recovered after this polarization modulation step increased by 113% compared to using only the spectral selection.

3.5.3 3rd Step: Image processing

On the best image obtained after the two acquisition steps (spectral selection and polarization modulation), the Dark Channel Prior (DCP) image processing tool was applied (Figure 25).

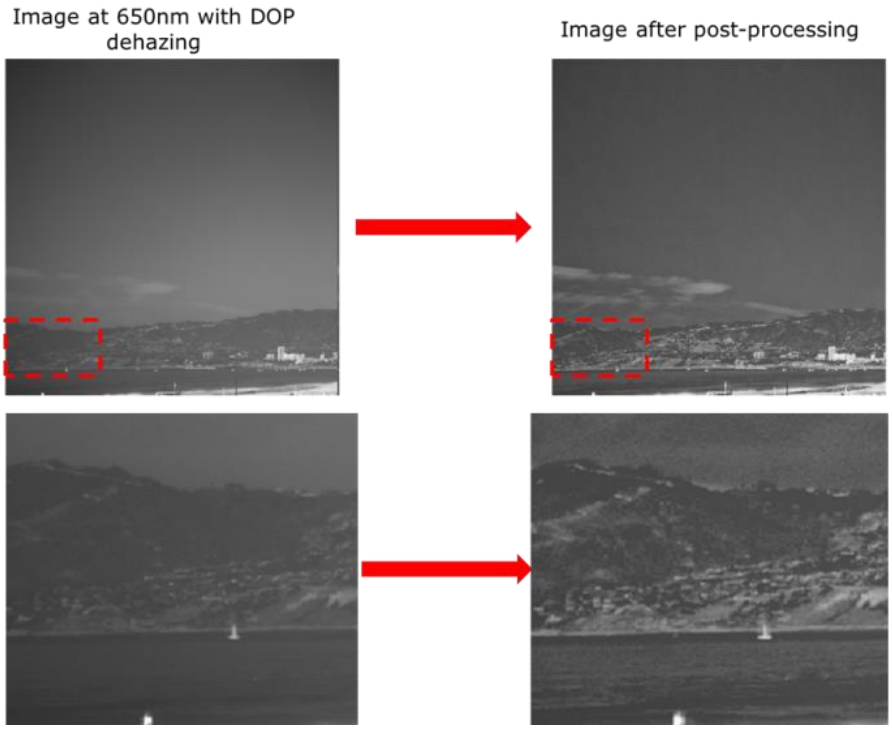

Figure 25: Best image obtained with spectral selection and polarization modulation technique with and without image dehazing. The last row is a zoom on the ROI area (red rectangle)

By using this technique, we have been able to increase by 3 times the number of edges recovered compared to using only the acquisition optimization steps.

4 Conclusion

During this phase I effort, successful demonstration have been done that a dehazing effect can be obtained by combining efficiently (Figure 26):

- Spectral selection
- Polarization modulation
- Image processing

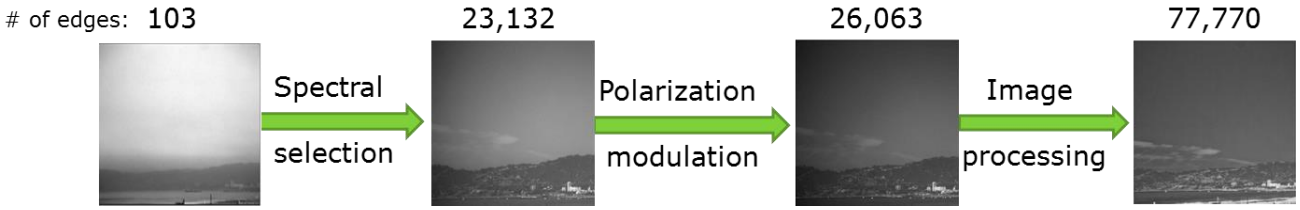

Figure 26: Decomposition of image dehazing processing

As it can be seen above, the two acquisition steps (spectral selection and polarization modulation) have allowed increasing significantly the quality of the image acquired. Then, the post-processing has been efficient to complete the dehazing process.

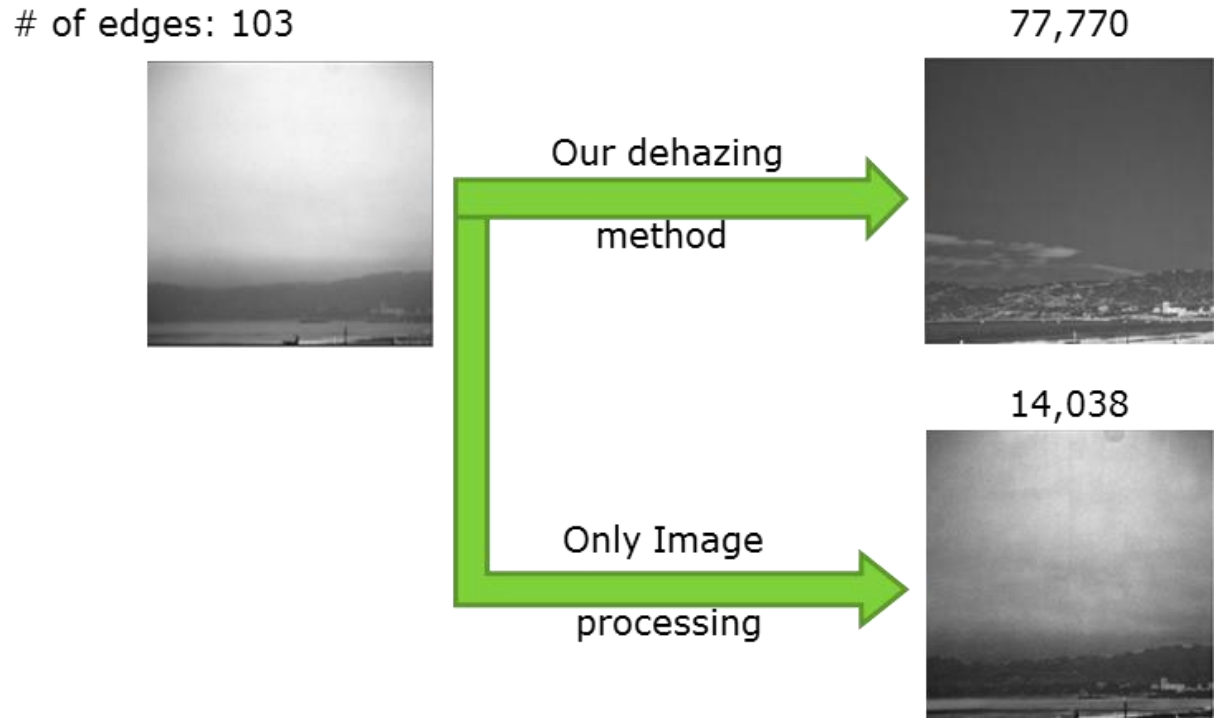

Figure 27: Comparison of the image obtained after our method and the one obtained using only image processing

This three step technique has permitted to increase notably the operational range of the imaging system technology compared to conventional method (figure 27). This has been quantified through the contrast of the scene: the number of edges detected has been increased **755 times compared to the same raw image acquired at 400nm** (Figure 27). It is an amelioration by a **factor 5.5 compared to using only post-processing techniques**.

We have successfully demonstrated that combined results of acquisition improvements and additional post-processing have increase drastically the image quality of outdoor scene in visible light.

5 Proposed Additional SBIR/STTR Funded Research

Three main guidelines have been determined for the phase Ib and phase II effort following the good results obtained during this phase I effort:

- On the spectral selection side, we have validated the importance of wavelength. For the fog used during our experiment we have been able to demonstrate that the best spectral wavelength to reduce haze effect is between red (650nm) and SWIR (1-3um). Our validated theory also pointed out that this best configuration will vary depending on fog condition. We propose for this reason to pursue and extend further our studies in SWIR, visible and NIR during a phase Ib and a phase II effort.
- On the polarization side, we have been able to validate various efficient methodologies. They present the advantage compared to other existing techniques to be fast (once implemented, the methods are instantaneous), robust and easy to implement. We propose for this reason to pursue this evaluation and technique characterization in visible and extend further our studies in SWIR and NIR during a phase Ib and a phase II effort.
- On the image processing side, many methods exist with their advantages and their inconvenient. The method used gives good dehazing results. However, it can in some case induce in noise and is not suitable for real time measurement (around 2minutes to process one image at a resolution of 1024x1024 pixels). To overcome those limitation, the next step planned for a phase Ib and phase II effort is to create a fog assessment algorithm (in order to reduce time when fog is not present) and combine it with an image processing technique (in order to use faster algorithm when it will improve or at least not degrade the dehazing process efficiency).

6 References

1. Bohren, Craig F. and Fraser, Alistair B. "At what altitude does the horizon cease to be visible?" *Am. J. Phys.* 54, 1986:222–227.
2. Henry, Ronald C.; Mahadev, Shudeish; Urquijo, Santiago and Chitwood, Derek. "Color perception through atmospheric haze." *J. Opt. Soc. Am. A* 17, 2000:831–835.
3. Chandrasekhar, Subrahmanyan. *Radiative Transfer*. pp. 24-37:280-284. New York: Dover Publications, 1960.
4. Harris, Daniel C, and Michael D. Bertolucci. *Symmetry and Spectroscopy: An Introduction to Vibrational and Electronic Spectroscopy*. New York: Oxford University Press, 1978
5. International Conference on the Properties of Water and Steam; Tremaine, Peter R. and International Association for the Properties of Water and Steam. *Steam, water, and hydrothermal systems : physics and chemistry meeting the needs of industry : proceedings of the 13th International Conference on the Properties of Water and Steam*. Ottawa: NRC Research Press, 2000.
6. Bohren, Craig F. and Huffman, Donald R. *Absorption and scattering of light by small particles*. New York: John Wiley & Sons, 1983.

7. Cullity, B D. *"Introduction to Magnetic Materials."* Reading, Mass: Addison-Wesley Pub. Co, 1972.
8. International Association for the Properties of Water and Steam. *"Release on the refractive index of ordinary water sub-stance as a function of wavelength, temperature and pressure*." IAPWS, 1997
9. Bertie, J. E. and Lan, Z. "*Infrared Intensities of Liquids XX: The Intensity of the OH Stretching Band of Liquid Water revisited, and the Best Current Values of the Optical Constants of H2O(l) at 25^{o}C between 15,000 and 1 cm^{-1}*." Applied Spectroscopy **50**, 1996
10. Henry, R. C.; Mahadev, S.; Urquijo, S. and Chitwood, D. *"Color perception through atmospheric haze."* J. Opt. Soc. Am. A **17**, 2000
11. Fattal, Raanan. *"Single image dehazing."* ACM SIGGRAPH 2008 papers, 2008
12. Narasimhan, S.G. and Nayar, S.K. *"Vision and the Atmosphere."* International Journal of Computer Vision **48**, 2002
13. Tan, R. T. *"Visibility in bad weather from a single image."* IEEE Conference on Computer Vision and Pattern Recognition, 2008
14. He, Kaiming; Sun, Jian and Tang, Xiaoou. *"Single Image Haze Removal Using Dark Channel Prior."*, IEEE Transactions on Pattern Analysis & Machine Intelligence **33**, 2010
15. Zhang, Yong-Qin et al. *"Visibility enhancement using an image filtering approach."* EURASIP J. Adv. Signal Process., 2012
16. Vedel, M., Breugnot, S. and Lechocinski, N., *"Full Stokes polarization imaging camera."* Proc. SPIE 8160, (2011).
17. D P. F. Fox and P. L. H. McSweeney, *"Dairy Chemistry and Biochemistry."* Blackie Academic & Professional, Chapman & Hall, London, 1998
18. Parodi, P. *"Milk fat in human nutrition."* Aust. J. Dairy Technol., 59:3-59, 2004
19. Calhoun, W. R. et al. *"Sensitive real-time measurement of the refractive index and attenuation coefficient of milk and milk-cream mixtures."* Journal of Dairy Science **93** (8), 2004
20. *"Milk fat size distribution by laser diffraction"* in Particle Characterization, Beckman Coulter, *www.coultercounter.com*
21. Tyo, J.S., Goldstein, D. L., Chenault, D. B., and Shaw, J. A., "Review of passive imaging polarimetry for remote sensing applications," Applied Optics 45 (22), 5453-5469 (2006).
22. Vedel, M., Breugnot, S. and Lechocinski, N., "Spatial calibration of Full stokes polarization imaging camera", Proc.SPIE 9099, (2014).
23. El Ketara, Mohamed et al., "Acquisition method improvement for Bossa Nova Technologies' full Stokes passive polarization imaging camera SALSA", Proc. SPIE 9853, 2016
24. Konnen, G. P. *"Polarized Light in Nature"*, CUP Archive, 1985
25. Yu, J. and Liao, Q. *"Fast single image fog removal using edge-preserving smoothing."* 2011 IEEE International Conference on Acoustics, Speech and Signal Processing (ICASSP), Prague, 2011
26. Hautiere, Nicolas et al. *"Blind contrast enhancement assessment by gradient ratioing at visible edges."* Image Analysis and Stereology Journal **27**, 2008

7 Appendix A: Key Terms

Key terms and acronyms used in the report in alphabetical order.

Airlight (or backscattered light): it is the light coming from the illumination source, scattered by the medium and going directly to the camera.

Atmospheric veil (or haze layer): it is expressed as $\boldsymbol{V(x,y) = A(1 - t(x,y))}$ where **A** is the global atmospheric light, **t** the transmission of the medium and **(x, y)** is pixels coordinates of the scene. It can be seen as a "veil" we are seeing through to observe a scene.

Degree of linear polarization (DOLP): it is a quantity used to describe the portion of an electromagnetic wave which is linearly polarized. A perfectly linearly polarized wave has a DOLP of 100%, whereas an un-polarized wave has a DOLP of 0%. It can be expressed using only the normalized stokes parameters s_1 and s_2: DOLP = $s_1 + s_2$.

Image processing: it is a post-processing dehazing method proposed in this report. It consists in reducing the haze effect after the image is acquired. Common technique involves applying low-pass filters and area recognition.

Normalized (or reduced) stokes parameters: set of the three Stokes parameters S_1, S_2 and S_3 normalized by the first Stokes parameter S_0. They are noted (s_1, s_2 and s_3) with $s_i = S_i / S_0$ for i=1, 2 and 3.

Performance metrics: Any metrics that can be used to quantify the efficiency of any dehazing method (in term of image recover and/or time processing). They can be classified in two categories: qualitative and quantitative. Qualitative methods are generally based on collection of human perception on the dehazing effect of a method compared to another one. Quantitative method can be absolute (no image reference needed) or relative (to an image dehazed). Absolute quantitative method includes for instance computational time evaluation or edge measurement. Relative method includes for instance contrast ratio measurement, Peak signal to noise ratio, mean square error.

Polarization modulation: it is a dehazing method proposed in this report. It consists in modulating the polarization response of the acquisition system in order to reduce haze effect. Common method used by photographers consists in using a simple polarizer.

Polarization of light: It is a parameter applying to electromagnetic waves that specifies the geometrical orientation of the electric field oscillation. It is with the intensity and the wavelength a parameter used to characterize completely light properties.

Spectral selection: it is a dehazing method proposed in this report. It consists in selecting specific wavelength in order to reduce haze effect.

Stokes parameters: set of four values (S_0, S_1, S_2 and S_3 also noted I, Q, U, and V) that describe completely the polarization state of an electromagnetic radiation. Simple mathematical operation allow from those values to determine parameter such as total intensity (I), (fractional) degree of polarization (DOP), and the shape parameters of the polarization ellipse.

Wavelength: it is the spatial period of the electromagnetic wave—the distance over which the wave's shape repeats.

8 Appendix B: Supplemental Data

a. Rayleigh scattering

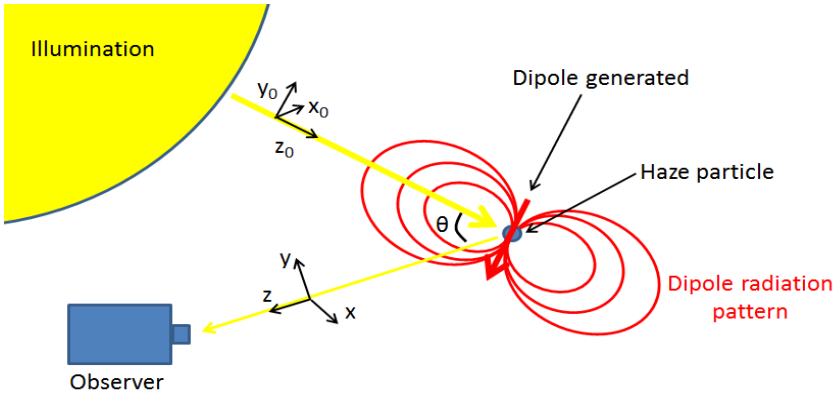

Figure 28: Scattering model in Rayleigh theory

In this regime $\alpha \ll 1$ which means that the particle is small enough compared to the wavelength so that the local electric field component of light is uniform at any instant.

This oscillating electric field induces an oscillating dipole due to the polarizability α_P of the particle:

$$\mathbf{p}(\mathbf{t}) = \alpha_P \mathbf{E_0}(\mathbf{t}) = \alpha_P (E_{0,x_0}(t)\,\mathbf{x_0} + E_{0,y_0}(t)\,\mathbf{y_0}) \quad (11)$$

with **p** dipole moment, $\mathbf{E_0}$ incident electric field and (x0, y0) Cartesian coordinates of the incident light.

Using the retarded scalar V_r and vector $\mathbf{A}_r$ potential, the radiated electric field can be expressed:

$$\mathbf{E_r}(\mathbf{r}, t) = -\nabla V_r(\mathbf{r}, t) - \partial_t \mathbf{A_r}(\mathbf{r}, t) \quad (12)$$

Where ∂_t (respectively ∂_{t^2}) is the first (respectively second) time derivative and ∇ is the gradient operator.

If we consider localized dipoles are in far-field (the observation point is far away from the haze particle), the relation can be rewritten:

$$\mathbf{E_r}(\mathbf{r}, t) = \frac{1}{4\pi}\left(-\nabla\left(\frac{1}{\varepsilon_0}\frac{\mathbf{r}.\mathbf{p}\left(t-\frac{\mathbf{r}}{c}\right)}{rc}\right) + \mu_0 \frac{\partial_{t^2}\left(\mathbf{p}\left(t-\frac{\mathbf{r}}{c}\right)\right)}{r}\right) = \frac{\mu_0}{4\pi r}\left[r\boldsymbol{e_r}\,\mathbf{x}\left(r\boldsymbol{e_r}\,\mathbf{x}\,\partial_{t^2}\left(\mathbf{p}\left(t-\frac{\mathbf{r}}{c}\right)\right)\right)\right] \quad (13)$$

where μ_0 the permeability, ε_0 the permittivity, c the speed of light and r the distance between the observer and the particle.

Using Eq.11, this equation can be written more explicitly in the coordinate of the observer by:

$$\mathbf{E_r}(\mathbf{x},\mathbf{y},\mathrm{t}) = \frac{\alpha_P \partial_{t^2}\left(\mathbf{E_0}\left(\mathrm{t}-\frac{\mathbf{r}}{\mathrm{c}}\right)\right)}{4\pi \mathrm{r} c^2}\frac{\sin\theta}{r}\boldsymbol{e_\theta} \quad \textbf{(14)}$$

With θ the scattering angle and $\boldsymbol{e_\theta}$ a unitary vector**.**

From this equation, we can conclude that this dipole will radiate at the same frequency as the applied field in all direction homogeneously.

Developing this equation, it is possible to express the resulting intensity of light emitted by one sphere particle with a diameter D in far field by the relation:

$$I(\lambda,\theta,z) = \left(\frac{2\pi}{\lambda}\right)^4\left(\frac{D}{2}\right)^6\left(\frac{n^2-1}{n^2+2}\right)^2\frac{1+\cos^2\theta}{2z^2}I_0 \quad \textbf{(15)}$$

with n the refractive index of the particle, I_0 the intensity of incident light on the particle, z the distance to the particle.

Integrating this equation on all angles, we can also determine the scattering cross section efficiency for this model $\sigma_{\mathrm{R-Scat}}$:

$$\sigma_{\mathrm{R-Scat}} = \frac{2\pi^5}{3}\frac{D^6}{\lambda^4}\left(\frac{n^2-1}{n^2+2}\right)^2 \quad \textbf{(16)}$$

To determine the degree of light polarization, we can express the light radiated by the particle in the observation coordinates:

$$\mathbf{E_r}(\mathbf{x},\mathbf{y},\mathrm{t}) = \frac{\alpha_P}{4\pi \mathrm{r c}^2}\left[-\partial_{t^2}\left(\mathbf{E}\left(\mathrm{t}-\frac{\mathbf{r}}{\mathrm{c}}\right)\right)\mathbf{x} + \cos\theta\,\partial_{t^2}\left(\mathbf{E}\left(\mathrm{t}-\frac{\mathbf{r}}{\mathrm{c}}\right)\right)\mathbf{y}\right] \quad \textbf{(17)}$$

Using the Stokes formalism, we can express the polarization light through different measurable intensities:

$$\boldsymbol{S_{detect}}(x,y,\lambda) = \begin{pmatrix} S_{0,detect} \\ S_{1,detect} \\ S_{2,detect} \\ S_{3,detect} \end{pmatrix} \quad \textbf{(18)}$$

with S_0 the total intensity of the light detected by the camera, S_1 the difference in intensities between the horizontal and vertical linearly polarized components, S_2 the difference in intensities between linearly polarized components traveling at 45° and −45° with respect to the x-axis; S_3 the difference in intensities between right and left circularly polarized light.

We can therefore express the degree of linear polarization as:

$$DOLP = \frac{\sqrt{S_1^2 + S_2^2}}{S_0} = \frac{\sqrt{(\|E_X\|^2 - \|E_Y\|^2) + (\|E_{+45}\|^2 - \|E_{-45}\|^2)}}{S_0} \quad (19)$$

If Eq.17 is inserted on Eq.19, we obtained the general relation for the degree of linear polarization:

$$DOLP = \frac{\sin^2\theta}{1 + \cos^2\theta} \quad (20)$$

This relation on the light polarization scattered by the particle is important since it gives direct relation between the geometry of the illumination-particle-observer scene and the polarization of light independently of the optical characteristics of the scatterer object (in the limit defined above).

b. Mie scattering

The Mie solution describes the scattering of an electromagnetic plane wave by a single homogeneous sphere using the Maxwell equations.

To use this model, there are some prerequisites:

1- The quantum mechanical effects are negligible and the physics can be described using classical electromagnetism equations (Maxwell equations).

2- Haze particles will be approximated by sphere (this approximation can be made due to the high surface tension of water).

3- The haze concentration is low enough to consider that interaction between particles is negligible (independent scattering): there is no interference between the waves scattered by each particles. This approximation is usually considered as obtained when the radius of one particle is 3 times less than the distance between one particle and another.

In this theoretical framework, we can apply the Maxwell equations for the two medium: the haze particle and the air. We can this way express the electric field through the Helmholtz equation:

$$\Delta \boldsymbol{E} + k^2 n^2 \boldsymbol{E} = \boldsymbol{0} \quad (21)$$

With *n* (respectively *k*) the index of refraction (resp. the angular wavenumber) in the medium considered.

a- Definition of vector and scalar potential

Since spherical object are the subject of interest, we can express this equation using only the scalar propagation in spherical coordinates (r, θ, φ):

$$\frac{\partial}{r^2 \partial r}\left(r^2 \frac{\partial \phi}{\partial r}\right) + \frac{1}{r^2 \sin\theta}\frac{\partial}{\partial \theta}\left(\sin\theta \frac{\partial \phi}{\partial \theta}\right) + \frac{1}{r^2 \sin^2\theta}\frac{\partial}{\partial \theta}\left(\sin\theta \frac{\partial^2 \phi}{\partial \varphi^2}\right) + k^2 n^2 \phi = 0 \quad (22)$$

With:

$$\boldsymbol{E} = \frac{1}{nk}\boldsymbol{\nabla}\mathrm{x}\,(nk\phi\boldsymbol{r}) + \frac{\mathrm{i}}{nk}\boldsymbol{\nabla}\mathrm{x}\left(\frac{1}{nk}\boldsymbol{\nabla}\mathrm{x}\,(nk\phi\boldsymbol{r})\right) \quad \textbf{(23)}$$

The electric field can also be expressed through the vector potential **A**:

$$\boldsymbol{E} = -\frac{\partial}{\partial t}\boldsymbol{A}(\boldsymbol{r},t) - \boldsymbol{\nabla}\phi(r,t) \quad \textbf{(24)}$$

Using the Faraday's law of induction:

$$\boldsymbol{\nabla}\mathrm{x}\,\boldsymbol{A}(\boldsymbol{r},t) = \frac{i}{\omega}\boldsymbol{\nabla}\mathrm{x}\,\boldsymbol{E} \quad \textbf{(25)}$$

Using Eq.17 and 19 the vector potential can be written as a linear combination of the electric field constitutive vectors:

$$\boldsymbol{A}(\boldsymbol{r},t) = \frac{i}{\omega}\sum_{a} X_a\,\boldsymbol{\nabla}\mathrm{x}\,(\phi\boldsymbol{r}) + Y_a\,\boldsymbol{\nabla}\mathrm{x}\left(\frac{1}{nk}\boldsymbol{\nabla}\mathrm{x}\,(\phi\boldsymbol{r})\right) \quad \textbf{(26)}$$

With X_a and Y_a constants.

b- Determination of scalar potential expression

We consider for this demonstration the case of a sphere with a diameter D, a complex refractive index $m = n + \mathrm{i}\kappa$ and a conductivity μ placed in a nonconductive environment (air) with a refractive index n_2=1.
An electromagnetic plane wave with wavelength is incident on the sphere.

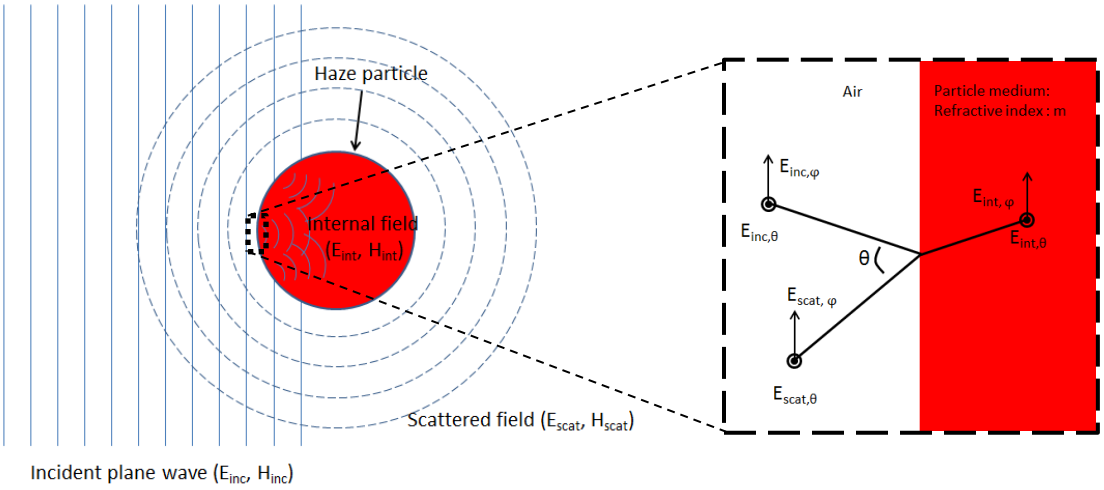

Figure 29: Scattering model in Mie theory

In this model, the incident and scattered waves are decomposed in spherical vectorial functions.
For simple geometry, the separation of variables technique can be used to solve this equation: the solution can be decomposed in three different functions with dependence in only r, θ or φ.

$$\phi(r,\theta,\varphi) = f(r)g(\theta)h(\varphi) \quad \textbf{(27)}$$

Using Eq.22 and 23, the solution can be expressed in series of Ricatti-Bessel function (where J_l and Y_l are the first order Bessel functions of respectively the first and second kind) and Legendre polynomials (where $P_l^{(m)}$ is the Legendre polynomial of l order and m kind) as:

$$\phi_o = \sum_{l=0}^{\infty}\sum_{m=0}^{l} a^{(m)}\sqrt{\frac{\pi}{2kr}}\left[x_l\, J_{l+\frac{1}{2}}(kr) + y_l\, Y_{l+\frac{1}{2}}(kr)\right] P_l^{(m)}(\cos\theta)\ \sin(m\varphi) \quad (28)$$

$$\phi_e = \sum_{l=0}^{\infty}\sum_{m=0}^{l} a^{(m)}\sqrt{\frac{\pi}{2kr}}\left[x_l\, J_{l+\frac{1}{2}}(kr) + y_l\, Y_{l+\frac{1}{2}}(kr)\right] P_l^{(m)}(\cos\theta)\cos(m\varphi)$$

With $a^{(m)}$, x_l, y_l constants and ϕ_o, ϕ_e odd and even scalar solutions.
In those equations, we can note that $Y_{l+1/2}$ is divergent in the limit r tend to 0 which is a non-physical solution so two case can be defined:
Inside the sphere: $y_l = 0$ (spherical Bessel functions).
Outside the sphere: we can select different parameters for x_l and y_l. Here we will use x_l=1 and y_l=-i (Hankel functions). It corresponds to an outgoing spherical wave pattern of the scattered field.

To simplify the notation, we introduce the parameter $z_l^{(1)}(kr) = \sqrt{\frac{\pi}{2kr}}\left[x_l\, J_{l+\frac{1}{2}}(kr) + y_l\, Y_{l+\frac{1}{2}}(kr)\right]$. The previous set of equation can now be rewritten as:

$$\phi_o = \sum_{l=0}^{\infty}\sum_{m=0}^{l} a_o^{(l,m)}\, z_l^{(1)}(kr)\, P_l^{(m)}(\cos\theta)\ \sin(m\varphi) \quad (29)$$

$$\phi_e = \sum_{l=0}^{\infty}\sum_{m=0}^{l} a_e^{(l,m)}\, z_l^{(1)}(kr)\, P_l^{(m)}(\cos\theta)\cos(m\varphi)$$

c- Determination of electric field expression
Maxwell equations states that:

$$\boldsymbol{E} = \frac{1}{-in^2k}\nabla\mathrm{x}(\boldsymbol{H}) = \frac{1}{-in^2k}\nabla\mathrm{x}\left(\frac{1}{i\omega\mu}\nabla\mathrm{x}\,\boldsymbol{A}(\boldsymbol{r},t)\right) \quad (30)$$

Using this equation and Eq.20, the incident fields can be written as:

$$\boldsymbol{E}_{inc} = \frac{k}{\omega^2\epsilon\mu}\sum_{l=0}^{\infty}\sum_{m=0}^{l} X_{l,m}\nabla\mathrm{x}\,(\phi\boldsymbol{r}) + Y_{l,m}\,\nabla\mathrm{x}\left(\frac{1}{nk}\nabla\mathrm{x}\,(\phi\boldsymbol{r})\right) \quad (31)$$

$$\boldsymbol{H}_{inc} = -i\frac{k}{\omega\,\mu}\sum_{l=0}^{\infty}\sum_{m=0}^{l} X_{l,m}\nabla\mathrm{x}\left(\frac{1}{nk}\nabla\mathrm{x}\,(\phi\boldsymbol{r})\right) + Y_{l,m}\nabla\mathrm{x}\,(\phi\boldsymbol{r})$$

With $X_{l,m}$ and $Y_{l,m}$ characteristic coefficient of the incident beam. For an incident plane wave, those coefficients can be calculated by integration around of the electric field around small area and is equal to:

$$X_{l,m} = \begin{cases} i^{l-1} E_0 \dfrac{2l+1}{l(l+1)}\ , & m = 1 \\ 0, & m \neq 1 \end{cases} \quad (32)$$

$$Y_{l,m} = iX_{l,m}$$

We can express with the same technique the scattered and internal fields:

$$\boldsymbol{E}_{scat} = \frac{k}{\omega^2 \epsilon \mu} \sum_{l=0}^{\infty} i^{l-1} E_0 \frac{2l+1}{l(l+1)} \left(a_l \boldsymbol{\nabla} \mathrm{x}\, (\phi \boldsymbol{r}) + i\, b_l \boldsymbol{\nabla} \mathrm{x} \left(\frac{1}{nk} \boldsymbol{\nabla} \mathrm{x}\, (\phi \boldsymbol{r}) \right) \right) \quad (33)$$

$$\boldsymbol{H}_{scat} = -i \frac{k}{\omega\, \mu} \sum_{l=0}^{\infty} i^{l-1} E_0 \frac{2l+1}{l(l+1)} \left(a_l \boldsymbol{\nabla} \mathrm{x} \left(\frac{1}{nk} \boldsymbol{\nabla} \mathrm{x}\, (\phi \boldsymbol{r}) \right) + i\, b_l \boldsymbol{\nabla} \mathrm{x}\, (\phi \boldsymbol{r}) \right)$$

$$\boldsymbol{E}_{int} = \frac{k}{\omega^2 \epsilon \mu} \sum_{l=0}^{\infty} i^{l-1} E_0 \frac{2l+1}{l(l+1)} \left(c_l \boldsymbol{\nabla} \mathrm{x}\, (\phi \boldsymbol{r}) + i\, d_l \boldsymbol{\nabla} \mathrm{x} \left(\frac{1}{nk} \boldsymbol{\nabla} \mathrm{x}\, (\phi \boldsymbol{r}) \right) \right)$$

$$\boldsymbol{H}_{int} = -i \frac{k}{\omega\, \mu} \sum_{l=0}^{\infty} i^{l-1} E_0 \frac{2l+1}{l(l+1)} \left(c_l \boldsymbol{\nabla} \mathrm{x} \left(\frac{1}{nk} \boldsymbol{\nabla} \mathrm{x}\, (\phi \boldsymbol{r}) \right) + i\, d_l \boldsymbol{\nabla} \mathrm{x}\, (\phi \boldsymbol{r}) \right)$$

with a_l, b_l the scattering coefficients and c_l and d_l the internal field coefficient.

More specifically, we can completely express the scattering electric field in the scattering plane using Eq. 29 and 31:

$$\boldsymbol{E}_{scat}(r, \theta, \varphi) = \frac{e^{ikr}}{ikr} \begin{pmatrix} 0 \\ -\cos\varphi\, S_2(\cos\theta) \\ \sin\varphi\, S_1(\cos\theta) \end{pmatrix} E_0 \quad (34)$$

With

$$S_1(\cos\theta) = \sum_{l=1}^{\infty} \frac{2l+1}{l(l+1)} \left(a_l\, \pi_l(\cos\theta) + b_l\, \tau_l(\cos\theta) \right)$$

$$S_2(\cos\theta) = \sum_{l=1}^{\infty} \frac{2l+1}{l(l+1)} \left(a_l\, \tau_l(\cos\theta) + b_l\, \pi_l(\cos\theta) \right)$$

with $\pi_l(\cos\theta) = \frac{\mathrm{dP_l^{(m)}}(\cos\theta)}{\mathrm{d}\,(\cos\theta)}$ and $\tau_l(\cos\theta) = \cos\theta \frac{\mathrm{dP_l^{(m)}}(\cos\theta)}{\mathrm{d}\,(\cos\theta)} - \sin^2\theta \frac{\mathrm{d^2P_l^{(m)}}(\cos\theta)}{\mathrm{d}\,(\cos\theta)^2}$.

d- Mie scattering parameters

To completely solve the scattering problem, it is necessary to find the four constants of the wave function equations: a_l, b_l, c_l and d_l.

To do so, using the Faraday's law to a small rectangular loop whose long sides run parallel to the interface between two materials we can determine that the tangential component of the electromagnetic field is continuous at an interface. Thus, the tangential component (cf. Figure 26) of the field inside the particle at the limit (r=D/2) is equal to the sum of the tangential components of the scattered and incident light field (**E** and **H**):

$$\begin{aligned} \boldsymbol{E}_{scat,\boldsymbol{\theta}} + \boldsymbol{E}_{inc,\boldsymbol{\theta}} &= \boldsymbol{E}_{int,\boldsymbol{\theta}} \\ \boldsymbol{H}_{scat,\boldsymbol{\theta}} + \boldsymbol{H}_{inc,\boldsymbol{\theta}} &= \boldsymbol{H}_{int,\boldsymbol{\theta}} \\ \boldsymbol{E}_{scat,\boldsymbol{\varphi}} + \boldsymbol{E}_{inc,\boldsymbol{\varphi}} &= \boldsymbol{E}_{int,\boldsymbol{\varphi}} \\ \boldsymbol{H}_{scat,\boldsymbol{\varphi}} + \boldsymbol{H}_{inc,\boldsymbol{\varphi}} &= \boldsymbol{H}_{int,\boldsymbol{\varphi}} \end{aligned} \quad (35)$$

We can then deduce the Mie coefficient for scattering and internal field:

$$a_l = \frac{\mathrm{m}^2\,\mathrm{j}_l(\mathrm{m}k\,D/2)[(\mathrm{k}\,D/2))\,\mathrm{j}_l(\mathrm{k}\,D/2)]' - \mu_1\mathrm{j}_l(\mathrm{k}\,D/2)[(\mathrm{m}k\,D/2)\mathrm{j}_l(\mathrm{m}k\,D/2)]'}{\mathrm{m}^2\,\mathrm{j}_l(\mathrm{m}k\,D/2)[(\mathrm{k}\,D/2))\,h_l^{(1)}(\mathrm{k}\,D/2)]' - \mu_1 h_l^{(1)}(\mathrm{k}\,D/2)[(\mathrm{m}k\,D/2)\mathrm{j}_l(\mathrm{m}k\,D/2)]'} \quad \textbf{(36)}$$

$$b_l = \frac{\mu_1\,\mathrm{j}_l(\mathrm{m}k\,D/2)[(\mathrm{k}\,D/2))\,\mathrm{j}_l(\mathrm{k}\,D/2)]' - \mathrm{j}_l(\mathrm{k}\,D/2)[(\mathrm{m}k\,D/2)\mathrm{j}_l(\mathrm{m}k\,D/2)]'}{\mu_1\,\mathrm{j}_l(\mathrm{m}k\,D/2)[(\mathrm{k}\,D/2))\,h_l^{(1)}(\mathrm{k}\,D/2)]' - h_l^{(1)}(\mathrm{k}\,D/2)[(\mathrm{m}k\,D/2)\mathrm{j}_l(\mathrm{m}k\,D/2)]'}$$

$$c_l = \frac{\mu_1\,\mathrm{j}_l(\mathrm{k}\,D/2)[(\mathrm{k}\,D/2))\,h_l^{(1)}(\mathrm{k}\,D/2)]' - \mu_1\,h_l^{(1)}(\mathrm{k}\,D/2)[(\mathrm{k}\,D/2)\mathrm{j}_l(\mathrm{k}\,D/2)]'}{\mu_1\,\mathrm{j}_l(\mathrm{m}k\,D/2)[(\mathrm{k}\,D/2))\,h_l^{(1)}(\mathrm{k}\,D/2)]' - h_l^{(1)}(\mathrm{k}\,D/2)[(\mathrm{m}k\,D/2)\mathrm{j}_l(\mathrm{m}k\,D/2)]'}$$

$$d_l = \frac{\mu_1\mathrm{m}\,\mathrm{j}_l(\mathrm{k}\,D/2)[(\mathrm{k}\,D/2))\,h_l^{(1)}(\mathrm{k}\,D/2)]' - \mu_1\mathrm{m}\,h_l^{(1)}(\mathrm{k}\,D/2)[(\mathrm{k}\,D/2)\mathrm{j}_l(\mathrm{k}\,D/2)]'}{\mathrm{m}^2\,\mathrm{j}_l(\mathrm{m}k\,D/2)[(\mathrm{k}\,D/2))\,h_l^{(1)}(\mathrm{k}\,D/2)]' - \mu_1 h_l^{(1)}(\mathrm{k}\,D/2)[(\mathrm{m}k\,D/2)\mathrm{j}_l(\mathrm{m}k\,D/2)]'}$$

With m complex refractive index of the particle and μ_1 the ratio of the magnetic permeability of the sphere to the magnetic permeability of the ambient medium (air)

e- Scattering efficiency and light polarization

Using Eq.34 and 36, it is possible to completely describe the scattering electric field and determine parameters such as:

- Scattering efficiency determined by integrating the scattered power over all directions:

$$Q_{scat} = \frac{2}{(k\,D/2)^2}\sum_{l=0}^{\infty}(2l+1)(|a_l|^2 + |b_l|^2)$$

- Scattered light polarization: Since we determine completely the light field, we can recover any polarization light information on the scattered light using this model.
- Other parameter could be of recover such as the absorption efficiency which are not presented in this report;

In fog, a photon can be scattered multiple time before reaching the detector. To describe this multiple scattering event, we need to introduce a new parameter the reduced scattering coefficient. It corresponds to the number of scatter event N observed during the propagation through a homogeneous scattering medium with a thickness d: $\mu_s' = N/d$ and can be expressed:

$$\mu_s' = \mu_s\,(1 - g)$$

With:

- g=<cos(θ)> the anisotropy of scattering defined with a probability of scattering in the forward direction and θ the angle of the scattered light with respect to the incident one: g=0 corresponds to isotropic scattering while $g \to 1$ corresponds to high probability of forward scattering and thus less diffusion in the medium composed of many spherical particles.
- μ_s correspond to the scattering coefficient of one particle and is defined as:

$$\mu_s = Q_{sca} \times \sigma_{particle} \times C_{particle}$$

Where:

Q_{sca} is the scattering efficiency

$\sigma_{particle}=\pi r^2$ is the geometrical cross section area of the particle (with r the radius of the particle)

$C_{particle}$ is the concentration of particle in the medium.

c. Polarization modulation

One of the causes of degradation in scattering medium is associated to airlight. Since the airlight is due to light scattered by small particles inside the medium, it depends on the distance between the object and the camera. To perform dehazing using polarization modulation, two assumptions have been made:

- Scattering will induce mainly additive airlight and attenuation of the signal of interest: we neglected any image blur or other effect.
- Light directly reflected by the object is mainly not polarized

The last approximation is valid for diffusive surface and can be assumed for specular surface far enough (figure 30).

The principle for dehazing is that images recovered are the addition of two images with different weight: an image of the scene without haze and an image composed of only airlight. The idea is to reduce the last component and maximize the first one. To do so, we present hereafter three different techniques based on polarization.

One virtual polarizer

Using the Stokes parameters measured with Bossa Nova Technologies' polarimetric camera, it is possible to contrast the effect induced by a perfect linear polarizer with that of the intensity observed with a standard camera ($S_{0,\ Polar}$). The light intensity image after a perfect linear polarizer which axis lies at φ angle with respect to a horizontal plane will be given by the relation:

$$\boldsymbol{S_{0,Polar}(x,y,\lambda) = \frac{\left(S_{0,detect}(x,y,\lambda) + \cos(2\phi)\, S_{1,detect}(x,y,\lambda) + \sin(2\phi)\, S_{2,detect}(x,y,\lambda)\right)}{2}} \quad \textbf{(37)}$$

Since we assumed the polarization light is only due to airlight, we can estimate the best configuration for the polarizer to have the highest dehazing effect by calculating the min $S_{0,\ polar}$ for any ϕ value.

Dehazing using Degree Of Polarization

The degree of polarization measured for a diffusive target is only due to the scattering medium. Thus, measuring only the non-polarized light component will remove partially the haze on the images acquired. This can be done using the Salsa camera through the relation:

$$\boldsymbol{S_{0,\ non-polar}(x,y) = S_{0,detect}(x,y) - \sqrt{S_1^2 + S_2^2 + S_3^2}} \quad \textbf{(38)}$$

The extended Degree of Polarization technique

In this dehazing technique, the idea is to remove the haze by first mapping the distance of the objects. The reason is that airlight intensity, A, depends on the fog distance between the viewer and the object through the relation:

$$\boldsymbol{A(z) = A_\infty \left[1 - e^{-\int_0^z \beta(u)du}\right]} \quad \textbf{(39)}$$

With β the coefficient of extinction due to scattering and absorption, $t(z) = e^{-\int_0^z \beta(u)du}$ the transmittance of incoherent light and A_∞ the airlight of an object which would be at an infinite distance.

The fog can be considered as homogeneous regarding the distance which means that we can rewrite the previous equation:

$$\boldsymbol{A(z) = A_{\infty}\left[1 - e^{-\beta z}\right] = A_{\infty}[1 - t(z)]} \quad \textbf{(40)}$$

The total intensity detected I_{detect} which will be seen by the viewer can be expressed:

$$\boldsymbol{I_{detect} = t(z)I_{object} + A(z)} \quad \textbf{(41)}$$

In the assumption considered here, only airlight is partially polarized. Thus, the airlight intensity component can be expressed for each pixel:

$$\boldsymbol{A(x,y) = DOP_{airlight}\, \Delta I(x,y)} \quad \textbf{(42)}$$

With ΔI the difference of light detected after a polarizer in two orthogonal configurations where the intensity of light detected are extremal and $DOP_{airlight}$ the degree of polarization of airlight.

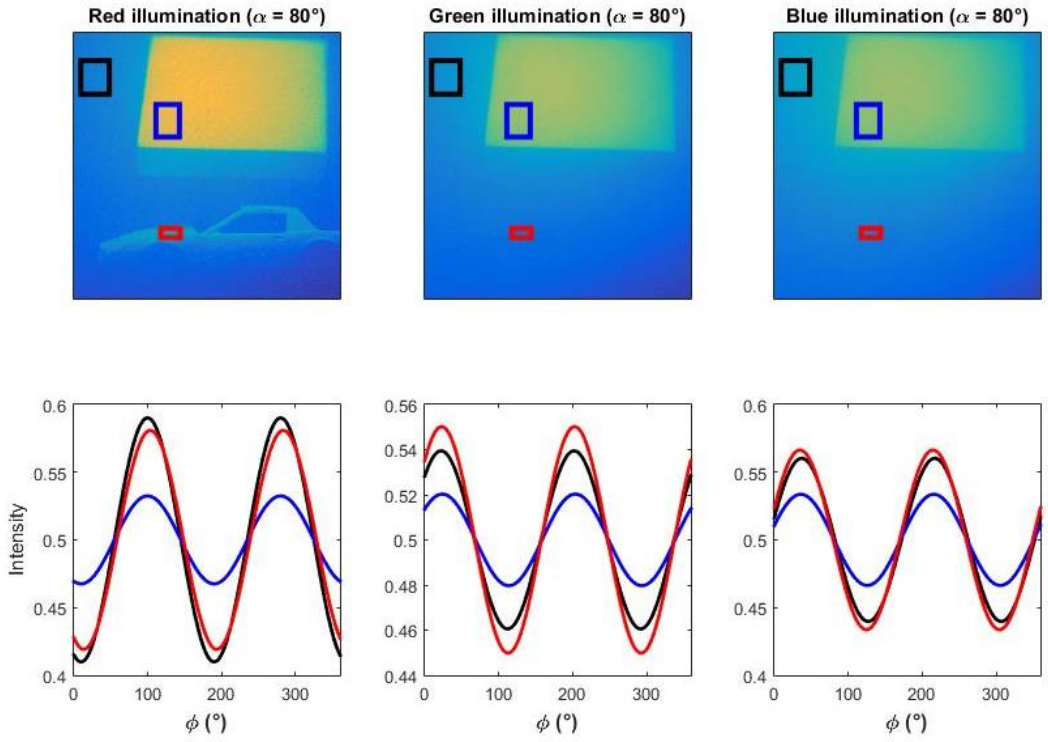

<u>Figure 30:</u> Evolution of intensities that would be obtained if a polarizer at an angle ϕ was placed in front of a camera (plotted lines on the charts) for different region of interest and different illuminations. The 3 rectangles represent the ROIs used to measure the intensities values. The volume concentration of milk in this experiment is 0.007%.

We can note in the figure above that the intensity detected and the value of ΔI are highly dependent of the part of the scene observed which can easily be understand since they depend on the object radiance observed and/or the transmittance of incoherent light through fog. However, we can note that the best and worst polarizations are found for the same polarizer angle. This is consistent with the approximation made at the beginning that light polarization is coming only from the light scattered by particle: light reflected by a specular object has no reason to be polarized at the same angle as light scattered by particle.

To dehaze the images, it is necessary to determine βz experimentally and so, A_∞ and $DOP_{airlight}$. Two heuristic methods can be used to determine those parameters, depending on the image content:

- There is a known point where only airlight is present (clear sky for example). In this case, A_∞corresponds directly to the measured intensity on this point and $DOP_{airlight}$ can directly be determined using Eq.42.
- There is the same object (for example same tree) in at least two different distance z_1 and z_2. This method can be generalized to known object taken on clear and hazing day.

In this report we use the first heuristic method to determine A_∞ and $DOP_{airlight}$. Then, the intensity of the object without haze can be expressed in each pixel as:

$$\boldsymbol{I_{object}(x,y) = \frac{I_{detect}(x,y) - DOP_{airlight}\,\Delta I(x,y)}{1 - A(x,y)/A_\infty}} \quad \textbf{(43)}$$

In this equation we can note that if there is no fog present, $I_{object}(x,y) = I_{detect}(x,y)$ since ΔI(x, y) will be equal to zero and $A(x,y) = A_\infty$.

d. Post-processing techniques

Many post-processing techniques are available. They generally differ on the filters used (bilateral filter, wiener filter …), the size of the filters, its adaptability and the speed of the image processing.
This section will be dedicated to the method used in this report: the Dark Chanel Prior Technique and more specifically when it is applied to a monochrome image.
As described in the *Multispectral polarization imaging solution- post processing techniques* section, the goal in this image post processing technique is to solve the under-constrained following equation:

$$I_{detect}(x,y) = J(x,y)t(x,y) + V(x,y) \quad \textbf{(44)}$$

With $\boldsymbol{V(x,y) = A(1 - t(x,y))}$

In order to find **J**, the idea is to determine first the atmospheric **V**.

The variation of the values of **V** is by definition dependent solely on the depth of the objects. Thus, objects with the same depth will have the same value of **V** and, in many situations it changes smoothly across small local areas. Thus, we can make the assumption that atmospheric veil has no specific edges or textures. So, the atmospheric veil from the hazy image can be recovered by applying a low pass filter to the image (texture being seen as noise). For this technique, the filter used is soft matting based on matting laplacien matrix. A bilateral filter is then applied to smooth small scall textures images.

Two heuristic methods can be used then to determine the airlight parameters for the monochrome image, depending on the image content:
- There is a known point where only airlight is present (clear sky for example). In this case, A_∞ corresponds directly to the measured intensity on this point and $DOP_{airlight}$ can directly be determined using Eq.42.
- There is the same object (for example same tree) in at least two different distance z_1 and z_2. This method can be generalized to known object taken on clear and hazing day.
In the experiments used, we used the first method: $I_{detect}(x_{sky}, y_{sky}) = A$
The image dehazed can be then expressed as:

$$J(x,y) = \frac{I_{detect}(x,y) - A(1 - t(x,y))}{\max(t(x,y), t_0)} \quad \textbf{(45)}$$

With t0 an arbitrary correction value (put to 0.1 in our case) in order to increase the visual intensity of the image observed.